Male-Biased Cyp17a2 Governs Antiviral Sexual Dimorphism in Fish via STING Stabilization and Viral Protein Degradation

Long-Feng Lu[a,c,1], Bao-jie Cui[a,e,1], Sheng-Chi Shi[a,c,1], Yang-Yang Wang[a,c], Can Zhang[a,c], Xiao Xu[a,e], Meng-Ze Tian[a,c], Zhen-Qi Li[a,c], Na Xu[a,c], Zhuo-Cong Li[a,c], Dan-Dan Chen[a,c], Li Zhou[a,c], Gang Zhai[a,c,2], Zhan Yin[f,a,c,2], Shun Li[a,b,c,d,e,2]

[a]Key Laboratory of Breeding Biotechnology and Sustainable Aquaculture, Institute of Hydrobiology, Chinese Academy of Sciences, Wuhan, Hubei 430072, China

[b]Laboratory for Marine Biology and Biotechnology, Qingdao Marine Science and Technology Center

[c]University of Chinese Academy of Sciences, Beijing, China

[d]Key Laboratory of Aquaculture Disease Control, Ministry of Agriculture, Wuhan, China

[e]College of Fisheries and Life Science, Dalian Ocean University, Dalian, China

[f]Key Laboratory of Mariculture, Ministry of Education, Ocean University of China, Qingdao 266003, China

[1]These authors have contributed equally to this work

[2]To whom correspondence may be addressed. Email: bob@ihb.ac.cn, zyin@ihb.ac.cn and zhaigang@ihb.ac.cn

Abstract

Differences in immunity between males and females in living organisms are generally thought to be due to sex hormones and sex chromosomes, and it is often assumed that males have a weaker immune response. Here we report that in fish, males exhibit stronger antiviral immune responses, which are driven by the male-biased gene Cyp17a2 rather than by hormones or sex chromosomes. First, we observed that male zebrafish exhibit enhanced antiviral resistance compared to females, and notably, zebrafish lack sex chromosomes. Through transcriptomic screening, we found that *cyp17a2* was specifically highly expressed in male fish. *Cyp17a2* knockout males were equivalent to wild-type males in terms of sex organs and androgen secretion, but the ability to upregulate IFN as well as antiviral resistance was greatly reduced. Then, Cyp17a2 is identified as a positive IFN regulator which located at endoplasmic reticulum, and specifically interacts with and enhances STING mediated antiviral responses. Mechanistically, Cyp17a2 stabiles STING expression by recruiting the E3 ubiquitin ligase bloodthirsty-related gene family member 32 (btr32), which facilitates K33-linked polyubiquitination. The capacity of IFN induction of Cyp17a2 was abolished when STING is knockdown. Meanwhile, Cyp17a2 also attenuates viral infection directly to strengthen the antiviral capacity as an antiviral protein, Cyp17a2 degrades the spring viremia of carp virus (SVCV) P protein by utilizing USP8 to reduce its K33-linked polyubiquitination. These findings reveal a sex-based regulatory mechanism in teleost antiviral immunity, broadening our understanding of sexual dimorphism in immune responses beyond the conventional roles of sex chromosomes and hormones.

Keywords

Cyp17a2; Sexual Dimorphism; STING; SVCV; Ubiquitination

Introduction

Research has demonstrated that innate immune responses to viruses differ significantly between the sexes. Males exhibit heightened susceptibility to viral pathogens, correlating with their generally weaker innate immune activation compared to females[1]. This immunological dimorphism manifests clinically as elevated infection intensity (quantified by intra-host viral load) and prevalence (population-level infection rates) in males[2]. Notably, sex-specific clinical outcomes are exemplified by severe acute respiratory syndrome coronavirus 2 (SARS-CoV-2) infections, where epidemiological data suggest males face twice the risk of intensive care unit (ICU) admission and a 30% higher mortality rate compared to females[3]. Similar trends extend to other viral pathogens including Dengue virus, hantaviruses, and hepatitis B/C viruses, all exhibiting male-biased infection prevalence[4, 5, 6].

Several factors have been identified as contributors to these sex-specific disparities in antiviral immunity, including hormonal variations and sex chromosomes. For instance, androgens such as testosterone exhibit broad immunosuppressive effects, including reduced NK cell cytotoxicity, impaired neutrophil chemotaxis, and attenuated macrophage proinflammatory cytokine production *in vitro*[7]. In addition, the Y chromosome harbors only two annotated miRNAs, while the X chromosome contains numerous immune-relevant miRNAs, and emerging evidence implicates X-escapee miRNAs as key modulators of sex-biased immune responses[8, 9].

It is well known that the interferon (IFN) response is an important host immune response to viral infection, in both mammals and fish[10]. The signaling pathways that activate IFN expression, although slightly different in fish and mammals, are generally conserved in both[11]. The endoplasmic reticulum (ER) protein stimulator of IFN genes (STING) is an important antiviral protein capable of resisting both DNA and RNA viruses by activating TANK binding kinase 1 (TBK1) during the induction of IFN production, which in turn phosphorylates IFN regulatory Factor 3 (IRF3) in the nucleus and activates the signaling of IFN transcription[12, 13]. For instance, STING deficiency has been shown to impair innate immune responses against multiple RNA viruses, such

as dengue virus, West Nile virus, and Japanese encephalitis virus[14, 15, 16]. Notably, oncogenes of the DNA tumor viruses, including human papillomavirus E7 and adenovirus E1A, function as potent and specific inhibitors of the cyclic GMP-AMP synthase (cGAS)-STING signaling pathway[17].

Cyp17a is classified within the cytochrome P450 (CYP450) family. In mammals, there is only one form, cyp17a1, which possesses both hydroxylase and lyase functions. Mutations in the human *cyp17a1* gene are associated with congenital adrenal hyperplasia (CAH)[18]. Comparative genomic analyses reveal that teleost fishes possess two distinct *cyp17a* isoforms, the evolutionarily conserved *cyp17a1* and a phylogenetically divergent *cyp17a2* paralog, with the latter representing a teleost-specific innovation absent in mammalian genomes[19]. Current investigations of Cyp17a2 in teleost species have predominantly centered on its mechanistic roles governing sexual development and differentiation, for example, with knockout of zebrafish *cyp17a2* leads to significant impairment of sperm motility[20]. Although Cyp17a2 has been characterized in sexual development, its non-canonical physiological roles have yet to be fully elucidated.

In most vertebrates, the XY sex chromosomes exhibit significant physiological differences between males and females, as exemplified in humans. However, the sex determination mechanisms in fish are more complex. For instance, zebrafish lack sex chromosomes, which confers a natural advantage. This absence allows for the exclusion of sex chromosome-related differences in the study of immunological disparities between males and females. Consequently, we selected zebrafish as the model organism for this investigation. This enabled us to more precisely identify the genes that are differentially expressed in male and female autosomes, which is crucial for understanding the immunological differences between the sexes. This study elucidates the role of the teleost-specific gene *cyp17a2* in antiviral immunity. Furthermore, the discovery that the male-biased expression of *cyp17a2* confers enhanced resistance to infection in males provides valuable insight into the complex mechanisms underlying sexual immune dimorphism.

Results

1. Male fish exhibit enhanced resistance to viral infection compared to female fish

To determine whether sex differences exist in the antiviral response capacity of fish, age-matched female and male zebrafish were intraperitoneally (i.p.) injected with SVCV. Male fish exhibited a significantly higher survival rate than female fish within seven days post-infection (Fig. 1A). Concurrently, females demonstrated a markedly higher incidence of cutaneous hemorrhages relative to males (Fig. 1B). Consistent with the reduced mortality, male fish showed less tissue damage in the liver and spleen following viral infection (Fig. 1C). IF analysis revealed that the SVCV N protein, represented by green fluorescence, was barely detectable in male tissues but was prominently present in female tissues (Fig. 1D). At the mRNA level, viral transcripts were quantified in these tissues, and the abundance of *svcv-n* gene was significantly lower in male tissues (Fig. 1E). At the protein level, SVCV N and G proteins were less frequently detected in male tissues compared to female tissues in 7 samples (Fig. 1F). Additionally, viral titers were significantly lower in the hearts of male fish compared to female fish (Fig. 1G). These findings demonstrate a stronger antiviral response capacity in male fish compared to female fish.

2. Male-biased gene cyp17a2 orchestrates antiviral immunity through RLR pathway

To explore the potential causes of the observed differences in virus resistance between male and female fish, transcriptome sequencing was performed on head-kidney tissues of healthy hermaphroditic adult zebrafish. Differential expression analysis identified 1511 upregulated genes and 1117 downregulated genes (Fig. 2A and Table S2). Among these, *cyp17a2* exhibits significant male-biased upregulation in eight sex-related genes, and it was confirmed by subsequent qPCR (Fig. 2B and S1A). Furthermore, we systematically quantified Cyp17a2 mRNA and protein expression in

145 multiple tissues of male and female zebrafish, demonstrating a consistent male-biased
146 expression pattern of Cyp17a2 (Fig. 2C and 2D). Thus, Cyp17a2 was selected for
147 further study. We first sought to understand whether it was associated with host antiviral
148 immunity, and the significant upregulation of the Cyp17a2 at the mRNA and protein
149 level in response to viral stimulation suggested its possible involvement in the antiviral
150 process (Fig. S1B and S1C). Following generation of *cyp17a2* knockout zebrafish,
151 previous study revealed that male *cyp17a2*$^{-/-}$ mutants displayed normal development of
152 male-typical secondary sexual characteristics comparable to WT males. However,
153 female *cyp17a2*$^{-/-}$ mutants exhibited significantly underdeveloped genital papillae
154 compared to their WT counterparts. To eliminate potential confounding effects of
155 androgen-mediated pathways on immune parameters, subsequent experiments were
156 conducted exclusively using male specimens from both genotypes. The male *cyp17a2*$^{-}$
157 $^{/-}$ mutants exhibited a higher mortality rate than WT males after viral infection (Fig. 2E).
158 Significant tissue damage and strong green fluorescence representing the SVCV N
159 protein was observed in the *cyp17a2*$^{-/-}$ tissues, virus titers assay also confirmed that
160 viral proliferation was higher in *cyp17a2*$^{-/-}$ group (Fig. S1D-S1F). Consistent with these
161 observations, the replication of viral genes transcription and protein levels were
162 increased in *cyp17a2*$^{-/-}$ homozygote tissues, these data demonstrated that Cyp17a2 is
163 crucial for host antiviral defense (Fig. 2F and S1G). To further understand their
164 functional mechanisms, a transcriptomic analysis contains total of 3,114 differentially
165 expressed genes (DEGs) were identified, there are 1,217 genes upregulated and 1,897
166 were downregulated in the liver of *cyp17a2* knockout male zebrafish compared to WT
167 males after viral infection (Fig. S1H). Kyoto encyclopedia of genes and genomes
168 (KEGG) pathway analysis revealed RIG-I-like receptors (RLRs), NOD-like receptors
169 (NLRs), and Toll-like receptors (TLRs) signaling pathways were significantly affected
170 (Fig. S1I). Gene set enrichment analysis (GSEA) showed that RLRs were
171 downregulated in *cyp17a2*$^{-/-}$ group under SVCV infection, combining with numerous
172 IFN-stimulated genes (ISGs) decreases (Fig. S1J and S2). To validate the transcriptome
173 data, *ifnφ1* levels were assessed and identified significantly downregulated in the
174 *cyp17a2*$^{-/-}$ group (Fig. 2G). Collectively, these data suggest that viral proliferation was

175 enhanced and IFN response were reduced in *cyp17a2*$^{-/-}$ fish.

176

177 **3. Cyp17a2 enhances IFN expression and suppresses viral proliferation**

178 Given the critical role of the IFN response in host defense against viral infections,
179 we investigated the impact of Cyp17a2 on IFN expression and viral infection *in vitro*.
180 Overexpression of Cyp17a2 significantly upregulated the IFN promoter and ISRE
181 activities in response to poly I:C or SVCV stimulation (Fig. 3A and S3A-S3B). An
182 effective sh-*cyp17a2*#2 was generated and confirmed at both the mRNA and protein
183 levels, and knockdown of *cyp17a2* inhibited both the IFN promoter and ISRE activity
184 (Fig. 3B-3E and S3C-S3D). RNA sequencing analysis of the cell line revealed that
185 SVCV infection activated numerous ISGs in Cyp17a2-overexpressing cells, whereas
186 these ISGs were significantly suppressed upon *cyp17a2* knockdown (Fig. 3F and Table
187 S3). The induction or attenuation of IFN and ISGs upon Cyp17a2 overexpression or
188 knockdown were confirmed by qPCR analysis, respectively (Fig. 3G and S3E). For
189 antiviral capacity assays, Cyp17a2 from zebrafish and gibel carp both inhibited the
190 proliferation of host-specific viruses, conversely, *cyp17a2* knockdown significantly
191 enhanced viral proliferation (Fig. 3H and S3F). Regarding viral mRNA and proteins,
192 overexpression or knockdown Cyp17a2 also displayed the similar opposite findings
193 (Fig. 3I-3J and S3G-S3H). IF assays indicated a lower intensity of green signals
194 representing the viral protein in the Cyp17a2 overexpression group compared to the
195 control, while a higher green signal was observed in the *cyp17a2* knockdown group
196 relative to the normal group (Fig. 3K and S3I). These results suggest that Cyp17a2
197 upregulates IFN expression and enhances antiviral capacity in the host.

198

199 **4. Cyp17a2 interacts with STING and stabilizes its expression**

200 Given the critical role of the RLR signaling pathway in fish IFN activation, the
201 relationship between Cyp17a2 and RLR signaling adaptors was investigated. Co-
202 transfection with Myc-Cyp17a2 and Flag-tagged RLR components (MAVS, TBK1,
203 STING, IRF3, IRF7) followed by anti-Flag immunoprecipitation identified specific
204 Cyp17a2-STING interaction via anti-Myc detection (Fig. 4A). Reciprocal Co-IP and

205 semi-endogenous IP assays confirmed this interaction (Fig. 4B and 4C). Truncated
206 STING mutants were generated to map binding domains (Fig. 4D). The transmembrane
207 domain (TM)-deficient STING-ΔTM-HA failed to bind Cyp17a2, indicating TM
208 domain dependence (Fig. 4E). Cyp17a2-GFP overlapped with ER markers in confocal
209 microscopy and colocalized with STING but failed to colocalize with the ΔTM mutant
210 (Fig. 4F-4G and S4A). To identify the effect of Cyp17a2 on STING regulation, the
211 mRNA level of sting was first analyzed, minimal change was observed in *sting* upon
212 Cyp17a2 overexpression (Fig. 4H). Protein-level studies demonstrated Cyp17a2
213 remarkably enhanced STING abundance and confirmed by confocal microscopy (Fig.
214 4I and S4B). Endogenous STING was similarly stabilized dependent on Cyp17a2
215 under untreated or stimulated conditions (Fig. 4J and S4C). Cycloheximide (CHX)
216 chase assay showed prolonged exogenous and endogenous STING half-life with
217 Cyp17a2 co-expression, and it was also confirmed by knockdown experiments (Fig.
218 4K and S4D-S4E). These data demonstrate that Cyp17a2 binds STING via its TM and
219 enhances STING posttranslational stability.
220
221 **5. Cyp17a2 enhances STING-mediated IFN expression and antiviral responses**
222 Considering that Cyp17a2 targets STING, a positive regulator of IFN production,
223 we investigated whether Cyp17a2 influences the IFN expression induced by STING.
224 The IFNφ1pro activity induced by STING overexpression was significantly
225 enhanced by Cyp17a2, with similar amplification observed for ISRE promoter
226 activation (Fig. 5A and S5A). Conversely, *cyp17a2* knockdown was shown to impair
227 STING-mediated IFNφ1pro and ISRE activation (Fig. 5B and S5B). Corresponding
228 increases in *ifn* and *vig1* transcripts were detected in Cyp17a2 overexpressing cells,
229 while Cyp17a2 knockdown suppressed these responses (Fig. 5C-5D and S5C-S5D).
230 The subsequent investigation focused on the potential modulatory effect of Cyp17a2
231 on the STING-induced cellular antiviral response. STING overexpression reduced
232 cytopathogenic effect (CPE), with viral titers decreased 336-fold compared to the
233 control group. This protection was augmented by Cyp17a2 co-expression, achieving an
234 additional 20-fold reduction (Fig. 5E and S5E). IB and IF analysis confirmed
235 that Cyp17a2 potentiated STING-mediated suppression of viral protein expression (Fig.

236 5F and S5F). SVCV gene transcripts were suppressed by STING, with enhanced
237 inhibition upon Cyp17a2 co-expression (Fig. 5G). STING dependency was
238 validated using shRNA knockdown (Fig. S5G). The antiviral capacity enhanced by
239 Cyp17a2 was markedly attenuated in cells with *sting* knockdown, as evidenced by
240 restored viral titers, gene and protein expression (Fig. 5H-5J and S5H-S5I). These
241 results demonstrate that Cyp17a2 potentiates STING activity to enhance IFN
242 production and antiviral responses.
243

244 **6. Cyp17a2 stabilizes STING through btr32-mediated K33-linked**
245 **polyubiquitination**

246 To elucidate the molecular mechanism by which Cyp17a2 augments STING
247 stabilization, proteasomal and lysosomal degradation were pharmacologically inhibited
248 using MG132 and Chloroquine (CQ), respectively. Accelerated STING degradation
249 caused by *cyp17a2* knockdown was rescued by MG132 but not CQ, suggesting
250 knockdown of *cyp17a2* promoted STING degradation via the proteasome pathway (Fig.
251 6A). Then, enhanced polyubiquitination of STING was detected upon Cyp17a2 co-
252 expression (Fig. 6B). Ubiquitin linkage analysis revealed selective enhancement of
253 K33-linked chains, with *cyp17a2* knockdown shown to reduce both WT and K33-
254 specific ubiquitination (Fig. 6C and S6A). Subsequently, candidate E3 ligases were
255 screened, revealing btr32 and SOCS3a as STING interactors (Fig. 6D). btr32 was
256 specifically identified as a Cyp17a2 binding partner through reciprocal Co-IP (Fig. 6E-
257 6G). Then the subcellular localization of btr32 was monitored, btr32-GFP signal
258 overlapped with the red signals of the ER marker, indicating that btr32 colocalizes with
259 the ER (Fig. 6H). Since the results identify that both STING and Cyp17a2 are localized
260 to the ER, btr32 was examined for cellular localization with both STING and Cyp17a2,
261 and the anticipated colocalization pattern was confirmed (Fig. 6I and 6J). Cyp17a2 was
262 found to strengthen btr32-STING interaction (Fig. 6K and S6B). Functional
263 assays demonstrated that btr32 augmented of Cyp17a2-mediated IFNφ1pro activity
264 and *vig1* mRNA induction (Fig. 6L and 6M). btr32 potentiated the Cyp17a2-dependent
265 stabilization of STING in both endogenous and exogenous systems (Fig. 6N). Two

266 shRNAs target btr32 were designed and generated, and after validating the knockdown
267 efficiencies for both endogenous and exogenous targets, sh-*btr32*#2 was selected for
268 the subsequent assay (Fig. S6C-S6D). The knockdown of btr32 impaired Cyp17a2-
269 enhanced STING activity, as shown by reduced IFNφ1pro response and *vig1* transcripts
270 (Fig. S6E and S6F). Additionally, *btr32* knockdown abolished Cyp17a2-mediated
271 STING upregulation in endogenous and overexpression system (Fig. S6G). These
272 findings establish that Cyp17a2 recruits btr32 to catalyze K33-linked
273 polyubiquitination, thereby stabilizing STING protein.
274
275 **7. STING K203 is essential for Cyp17a2-mediated ubiquitination**
276 The mechanism between btr32 and Cyp17a2 in STING stabilization was further
277 characterized. btr32 overexpression was shown to intensify Cyp17a2-driven STING
278 ubiquitination, while *btr32* knockdown attenuated this effect (Fig. 7A and S7A).
279 Specific enhancement of K33-linked ubiquitination by btr32 was demonstrated, with
280 reciprocal reduction upon btr32 abrogation (Fig. 7B and S7B). Mass spectrometry
281 analysis identified K203 and K221 as candidate ubiquitination sites (Fig. 7C). Among
282 generated lysine-to-arginine mutants (K203R, K221R), STING stabilization by
283 Cyp17a2 was abolished specifically in K203R mutant (Fig. 7D). Corresponding loss of
284 IFN induction and ubiquitination capacity were observed in K203R mutant (Fig. 7E-
285 7G). K33-linked ubiquitination was specifically impaired in K203R but not K221R
286 variants (Fig. S7C). btr32-mediated enhancement of WT and K33-specific
287 ubiquitination was eliminated in K203R mutant (Fig. 7H and S7D). btr32 domain
288 analysis was performed using RING/BBOX/SPRY deletion mutants (Fig. 7I). The
289 SPRY domain was required for btr32-STING-Cyp17a2 interactions (Fig. 7J-7L). Both
290 RING and SPRY domains were essential for btr32-driven ubiquitination (Fig. 7M and
291 S7E). These data establish K203 as the critical ubiquitination site in STING and define
292 RING/SPRY domains of btr32 as necessary for Cyp17a2-mediated stabilization.
293
294 **8. Cyp17a2 Degrades SVCV P Protein Through Modulation of K33-Linked**
295 **Polyubiquitination**

To determine whether Cyp17a2 directly engage in antiviral activity beyond regulating host immune responses, Co-IP assays were performed. Transient transfection experiments revealed specific interaction between Cyp17a2 and SVCV P protein, which was confirmed reciprocally (Fig. 8A and 8B). This interaction was further observed in SVCV-infected cells using P protein-specific antibody (Fig. 8C). In our antiviral trials, overexpression of Cyp17a2 led to a reduction in P protein levels during SVCV infection. Consequently, the investigation focused on whether Cyp17a2 could directly target the SVCV P protein for degradation. As anticipated, the co-expression of Cyp17a2 resulted in a decrease in the level of SVCV P protein Overexpression of Cyp17a2 reduced P protein levels during SVCV infection (Fig. 8D). Fluorescence microscopy confirmed diminished red fluorescent signals corresponding to SVCV P protein in Cyp17a2-expressing cells (Fig. 8E). Confocal microscopy analysis of SVCV P protein subcellular distribution revealed that the fluorescent signals from P-mCherry fusion constructs (red) showed partial co-localization with Cyp17a2 (green) in cytoplasmic compartments (Fig. 8F). To investigate degradation mechanisms, inhibitors targeting distinct pathways were tested. Cyp17a2-mediated P protein degradation was blocked by the proteasome inhibitor MG132, but not by autophagy inhibitors (3-MA, Baf-A1, CQ) (Fig. 8G). Ubiquitination assays demonstrated that Cyp17a2 significantly reduced P protein polyubiquitination (Fig. 8H). Mutation analysis using ubiquitin variants revealed that Cyp17a2 selectively decreased K33-linked polyubiquitination, as K33R mutants exhibited no significant changes, while K33-specific ubiquitination was markedly reduced (Fig. 8I and 8J). In contrast, knockdown of *cyp17a2* exhibited minimal impact on both WT-Ub and K33-linked polyubiquitination levels of the P protein (Fig. 8K). These findings demonstrate that Cyp17a2 promotes proteasomal degradation of the SVCV P protein by selectively attenuating K33-linked polyubiquitination, defining its role as an antiviral protein.

9. The K12 site of P protein is essential for Cyp17a2-mediated degradation

To investigate the specific molecular mechanism underlying ubiquitination-mediated degradation of the P protein, mass spectrometry analysis revealed ubiquitin-specific protease 7 (USP7) and USP8 as candidate deubiquitinating enzymes (Fig. 9A). Both USP7 and USP8 were found to associate with the P protein, however, only USP8 interacted with Cyp17a2. Therefore, USP8 became the focus of subsequent study (Fig.

329 9B and 9C). The validity of these interactions was further confirmed through reciprocal
330 experiments (Fig. S8A). Confocal microscopy analysis of USP8 subcellular
331 localization demonstrated overlapping cytoplasmic co-localization between USP8-GFP
332 (green fluorescence) and mCherry-tagged Cyp17a2 or the P protein (red fluorescence)
333 (Fig. 9D and S8B). Cyp17a2 overexpression enhanced USP8 and P protein binding,
334 whereas *cyp17a2* knockdown disrupted this interaction (Fig. 9E and S8C). USP8
335 overexpression amplified Cyp17a2-mediated P protein reduction (Fig. 9F). Knockdown
336 of USP8 abolished Cyp17a2-dependent P protein degradation (Fig. 9G and S8D). USP8
337 facilitated Cyp17a2-induced deubiquitination of P protein, with knockdown reversing
338 this effect (Fig. 9H and S8E). This result was also observed in the K33-linked
339 ubiquitination assay (Fig. 9I and S8F). Mass spectrometry identified K12 as a critical
340 lysine modification site (Fig. 9J). The K12R mutant resisted Cyp17a2-mediated
341 degradation and showed impaired deubiquitination in WT ubiquitin and K33-linked
342 assays (Fig. 9K-9L and S8G). USP8 failed to enhance Cyp17a2-mediated
343 deubiquitination in K12R mutants (Fig. 9M and S8H). Truncation analysis
344 demonstrated that USP8 residues 1-301 aa or 734-1067 aa were essential for
345 interactions with P protein and Cyp17a2 (Fig. 9N and 9O). USP8 mutants only residues
346 1-301 aa or 302-733 aa lost the ability to support Cyp17a2-mediated P protein
347 deubiquitination (Fig. 9P and S8I). These data establish that Cyp17a2 requires USP8
348 and the P protein K12 site to mediate deubiquitination-dependent degradation, with
349 USP8 residues 734-1067 aa being indispensable for this process.

350 **Discussion**

351 The influence of biological sex on antiviral immunity shows both evolutionary
352 parallels and divergences across species. While mammals typically exhibit stronger
353 female immunity through sex chromosome and hormonal mechanisms, our study
354 reveals an intriguing reversal in zebrafish, where males show enhanced antiviral
355 responses via an autosomal gene-mediated pathway. This supplements conventional
356 views and highlights the evolutionary plasticity of teleost immune systems.

357 Teleost display remarkable diversity in sex determination mechanisms, including

358 XX/XY, ZZ/ZW, and environmental systems[21, 22, 23]. This diversity provides a unique
359 framework for studying sexual dimorphism independent of sex chromosomes. Using
360 zebrafish, which lack conserved sex chromosomes, allows us to exclude the
361 confounding effects of divergent sex-chromosome gene dosage and focus on the role
362 of autosomal genes and their differential regulation in shaping sex-biased immunity.
363 Our study leverages this unique context to demonstrate that enhanced antiviral
364 immunity in males is driven not by canonical sex chromosomes or hormones, but by
365 the male-biased expression of the autosomal gene *cyp17a2*.

366 Mechanistically, Cyp17a2 operates through dual antiviral pathways, it stabilizes
367 STING via btr32-mediated K33-linked ubiquitination, enhancing IFN production, and
368 recruits USP8 to remove K33-linked chains from viral P protein, promoting its
369 degradation (Fig. 10). This establishes Cyp17a2 as a central regulator of sex-specific
370 antiviral immunity independent of sex chromosome pathways. Particularly noteworthy
371 is the demonstration that sexual dimorphism in immunity can arise through differential
372 regulation of autosomal genes rather than direct sex chromosome effects - a mechanism
373 distinct from mammalian X-linked immune gene dosage effects or estrogen-mediated
374 immunomodulation.

375 A key question emerging from our findings is whether the Cyp17a2-mediated
376 antiviral mechanism is conserved across the teleost lineage or represents an adaptation
377 specific to cyprinids such as zebrafish. The teleost-specific nature of *cyp17a2* suggests
378 functions shaped by aquatic environmental challenges. While further studies in diverse
379 teleost families are needed, the presence of *cyp17a2* orthologs across fish genomes
380 indicates potential conservation. It is proposed that the recruitment of a core component
381 of the steroidogenic enzyme machinery into the innate immune network may represent
382 a significant evolutionary adaptation in teleost. Aquatic environments have been shown
383 to have a persistently high pathogen load. The co-option of a gene such as *cyp17a2*,
384 which is already subject to sex-biased regulatory control, offers an efficient and rapidly
385 deployable strategy for establishing sexually dimorphic immunity, obviating the
386 necessity for de novo evolution of entirely new pathways.

387 Sexual dimorphism in viral susceptibility represents a conserved yet

mechanistically complex phenomenon across vertebrates[24]. While males generally exhibit increased vulnerability to numerous viral pathogens such as dengue virus and influenza A virus, notable exceptions exist where females demonstrate higher susceptibility, including infections by herpes simplex virus and measles virus[2]. These divergent patterns underscore a dual dependency of sex-biased infection outcomes on both host immunological determinants and viral evolutionary strategies[1]. For instance, the male predominance observed in severe dengue virus cases may be explained by both gender-specific occupational exposure risks and sexual dimorphism in Ab-dependent enhancement mechanisms, potentially linked to androgen-mediated modulation of antiviral immune responses[25]. Whereas female susceptibility to herpes simplex virus could be related to ovarian sex hormones, including estradiol and progesterone[26]. Critically, sex differences in antiviral immunity are not static but evolve across the lifespan and are tightly linked to age and reproductive status[27]. For example, sex disparities in hantavirus infection outcomes emerge post-puberty, coinciding with hormonal maturation[28]. Similarly, during the 2009 H1N1 pandemic in Japan, morbidity rates exhibited a triphasic sex bias: males<20 and >80 years old showed higher susceptibility than females, whereas females of reproductive age (20-49 years) faced elevated risks[29]. This pattern aligns with the hypothesis that estrogen peaks during reproductive years enhance antiviral defenses in females, while age-related declines in gonadal hormones may diminish this protective effect in postmenopausal populations[30]. Our study extends these principles to teleost species, revealing novel sex-specific resistance patterns in fish-virus interactions. Male zebrafish demonstrated heightened resistance to SVCV, while male crucian carp exhibited reduced susceptibility to CyHV-2[31]. These findings suggest that male-biased resistance may represent an evolutionarily conserved strategy in certain fish-virus system. This may reflect evolutionary adaptations to unique aquatic pressures. We propose several non-mutually exclusive hypotheses, which are rooted in the unique life histories and ecological pressures faced by aquatic vertebrates[32]. Firstly, the aquatic environment acts as a potent reservoir for pathogens, constantly exposing fish to diverse microbial challenges. This high pathogen pressure may select for specialized and potent immune strategies. If males and females encounter different levels or types of parasites or infections due to their behavior or morphology, this could lead to the evolution of sex-specific immune adaptations. Secondly, this phenomenon can be viewed through the lens of life-history trade-offs. Investment in immunity is costly in terms of energy and must be balanced against other

422 demands, such as reproduction. In many teleost species, male reproductive success
423 depends heavily on courtship displays, nest guarding and aggressive competition with
424 other males, all of which are high-energy activities that can compromise immune
425 function. Finally, the prevalence of external fertilization in teleost is a crucial factor.
426 Unlike mammals, where the embryo develops internally and is protected by the
427 maternal immune system, fish embryos are exposed to the pathogen-rich aquatic
428 environment from the moment of fertilization. Therefore, a male's contribution to
429 offspring survival includes not only his genetic material, but also the intrinsic pathogen
430 resistance of his sperm and the antimicrobial properties of the seminal fluid or nest site.
431 STING was originally identified as a critical adaptor molecule mediating antiviral
432 signaling cascades[33, 34]. Subsequential studies have established its indispensable role in
433 orchestrating innate immune responses against both DNA and RNA viral pathogens.
434 Current mechanistic understanding reveals that upon detection of cytoplasmic
435 pathogen-derived DNA, STING operates through two distinct molecular pathways:
436 serving as a downstream effector of essential single-stranded/double-stranded DNA
437 sensors or functioning as a direct receptor for microbial cyclic dinucleotides (CDNs).
438 Following activation, this TM protein recruits and activates TBK1, which subsequently
439 phosphorylates IRF3 to facilitate its nuclear translocation and initiate IFN production.
440 Notably, the protein demonstrates functional pleiotropy in RNA viral infections through
441 selective interaction with RIG-I rather than melanoma differentiation-associated
442 protein 5 (MDA5), thereby activating parallel IRF3-dependent antiviral signaling
443 pathways. Numerous studies indicate remarkable conservation of STING-mediated
444 IFN induction mechanisms across teleost species[35, 36, 37]. Mechanism studies further
445 reveal that fish STING maintains dual antiviral functionality against both nucleic acid
446 virus types, while simultaneously being subjected to targeted manipulation by various
447 viral pathogens as an immune evasion strategy.
448 Beyond its steroidogenic functions, Cyp17a2 represents a novel scaffold protein
449 in ubiquitination pathways. Despite the absence of clearly identifiable domains that are
450 directly implicated in ubiquitination (e.g., RING, HECT, or U-box domains), it is
451 proposed that the subcellular localization and protein-interaction capability of Cyp17a2
452 are pivotal to its novel function. As an ER-resident protein, Cyp17a2 is strategically co-
453 localized with central innate immune sensors such as STING. This shared localization
454 facilitates specific protein-protein interactions, enabling Cyp17a2 to serve as an
455 essential platform that recruits the E3 ubiquitin ligase btr32 to stabilize STING via K33-

linked ubiquitination. In contrast, Cyp17a2 engages the deubiquitinate USP8 to remove K33-linked chains from the viral P protein, thereby targeting it for degradation. This bifunctional and scaffolding role, which orchestrates both the addition and removal of specific ubiquitin chains to fine-tune antiviral responses, represents a fascinating evolutionary adaptation in teleost.

The CYP450 enzyme superfamily exhibits multifaceted roles across species, encompassing physiological processes and immune regulation. In human immune cells, pharmacological inhibition of CYP1A has been demonstrated to upregulate the expression of stem cell factor receptor and interleukin 22, directly linking CYP1-dependent metabolism of environmental small molecules to immune modulation[38]. Evolutionary conservation of this regulatory mechanism is evident in teleost, where grass carp (*Ctenopharyngodon idella*) CYP1A demonstrates dynamic expression during grass carp reovirus (GCRV) infection, implicating its role in antiviral immunity[39]. Our study further identifies Cyp17a2 as a sexually dimorphic regulator of IFN signaling in fish. This finding expands the recognized roles of the CYP450 superfamily in immune regulation, revealing a novel mechanism underlying sex-specific immunity in lower vertebrates.

In conclusion, zebrafish model with its lack of conserved sex chromosomes and environmental sex determination plasticity, provides unique insights into the evolutionary continuum of sexual dimorphism. Our results suggest that the relationship between sexual differentiation and immune competence may be more fluid in teleost than in mammals, potentially reflecting adaptive responses to aquatic pathogens and variable mating systems. Future investigations should explore whether this autosomal-centered mechanism represents a teleost specific adaptation or an ancestral feature subsequently modified in terrestrial vertebrates, while also examining potential interactions between environmental sex determinants and immune gene regulation.

Acknowledgment

We thank Fang Zhou (Institute of Hydrobiology, Chinese Academy of Sciences) for assistance with confocal microscopy analysis and Dr. Feng Xiong (China Zebrafish Resource Center, Institute of Hydrobiology, Chinese Academy of Sciences) for assistance with qPCR analysis.

This work was supported by the Strategic Priority Research Program of the Chinese Academy of Sciences (XDB0730300), Biological Breeding-National Science and Technology Major Project (2023ZD04065), National Excellent Youth Science Fund (32322086) and the Youth Innovation Promotion Association provided funding to Shun Li. National Key Research and Development Program of China (2023YFD2400201) provided funding to Dan-Dan Chen. National Natural Science Foundation of China (32173023) provided funding to Long-Feng Lu.

Declaration of interests

The authors declare no competing interests.

STAR Methods

Ethics statement

The experiments involved in this study were conducted in compliance with ethical regulations. The fish experiments were carried out under the guidance of the European Union Guidelines for the Handling of Laboratory Animals (2010/63/EU) and approved by the Ethics Committee for Animal Experiments of the Institute of Hydrobiology, Chinese Academy of Sciences (CAS) (No. 2024-069).

Fish, cells, and viruses

Mature zebrafish individuals 2.5 months after hatching (0.4 ± 0.1 g) were selected in this study. Wild-type (WT) zebrafish (AB strain; *Danio rerio*) were procured from the China Zebrafish Resource Center (CZRC), while *cyp17a2* mutant lines were generously provided by Dr. Zhan Yin's laboratory at the Institute of Hydrobiology, Chinese Academy of Sciences. All specimens were bred using standardized procedures. In accordance with the ethical requirements and national animal welfare guidelines, all experimental fish were required to undergo a two-week acclimatization period in the laboratory and have their health assessed prior to the commencement of the study. Only fish that appeared healthy and were mobile were selected for scientific investigation.

517 ZF4 cells (American Type Culture Collection, ATCC) were cultured in Ham's F-12
518 medium (Invitrogen) supplemented with 10% fetal bovine serum (FBS) at 28˚C and 5%
519 CO_2. EPC cells were obtained from the Chinese Culture Collection Centre for Type
520 Cultures (CCTCC), Gibel carp brain (GiCB) cells were provided by Ling-Bing Zeng
521 (Yangtze River Fisheries Research Institute, Chinese Academy of Fishery Sciences),
522 these cells were maintained at 28°C in 5% CO_2 in medium 199 (Invitrogen)
523 supplemented with 10% FBS. Spring viremia of carp virus (SVCV) was propagated in
524 EPC cells until a CPE was observed, and then cell culture fluid containing SVCV was
525 harvested and centrifuged at 4×10^3 *g* for 20 min to remove the cell debris, and the
526 supernatant was stored at -80°C until used. Cyprinid herpesvirus 2 (CyHV-2, obtained
527 from Yancheng city, Jiangsu province, China) was provided by Prof. Liqun Lu
528 (Shanghai Ocean University). CyHV-2 was propagated in GICB cells and harvested in
529 a similar way to SVCV.

530 **Plasmid construction and reagents**

531 The sequences of zebrafish and gibel carp (*Carassius gibelio*) Cyp17a2 (GenBank
532 accession number: NM_001105670.1 and XM_026199804.1) were obtained from the
533 National Centre for Biotechnology Information (NCBI) website. Cyp17a2 was
534 amplified by polymerase chain reaction (PCR) using cDNA from adult zebrafish or
535 gibel carp tissues as a template and cloned into the expression vector pCMV-HA or
536 pCMV-Myc (Clontech) vectors. Zebrafish MAVS (NM_001080584.2), TBK1
537 (NM_001044748.2), STING (NM_001278837.1) and the truncated mutants of STING,
538 IRF3 (NM_001143904.1), IRF7 (BC058298.1), btr32 (XM_021470074.1) and the
539 truncated mutants of btr32, TRAIP (NM_205607.1), SOCS3a (NM_199950.1), USP7
540 (XM_021473871.1), USP8 (XM_009293353.4), and N, P, and G protein (DQ097384.2)
541 of SVCV were cloned into pCMV-Myc and pCMV-Tag2C vectors. The shRNA of
542 *Pimephales promelas* Cyp17a2 (XM_039679078.1), STING (HE856620.1), and USP8
543 (XM_039680290.1) were designed by BLOCK-iT RNAi Designer and cloned into the
544 pLKO.1-TRC Cloning vector. For subcellular localization experiments, Cyp17a2 was
545 constructed onto pEGFP-N3 (Clontech), while STING and P protein were constructed
546 onto pCS2-mCherry (Clontech). The plasmids containing zebrafish IFNφ1pro-Luc and

547 ISRE-Luc in the pGL3-Basic luciferase reporter vector (Promega) were constructed as
548 described previously. The *Renilla* luciferase internal control vector (pRL-TK) was
549 purchased from Promega. The ubiquitin mutant expression plasmids Lys-33/63 (all
550 lysine residues were mutated except Lys-33 or Lys-63) and Lys-33R/63R (only Lys-33
551 or Lys-63 mutated) were ligated into the pCMV-HA vectors named Ub-K33O/K63O-
552 HA and Ub-K33R/K63R. All constructs were confirmed by DNA sequencing.
553 Polyinosinic-polycytidylic acid (poly I:C) was purchased from Sigma-Aldrich used at
554 a final concentration of 1 μg/μl. MG132 (Cat. No. M7449), 3-Methyladenine (3-MA)
555 (Cat. No. M9281), CQ (Cat. No. C6628) were obtained from Sigma-Aldrich.
556 Bafilomycin A1 (Baf-A1) (Cat. No. S1413) and CHX (NSC-185) were obtained from
557 Selleck.

558 **Transcriptomic analysis**

559 Total RNA was extracted using the TRIzol method and evaluated for RNA purity
560 and quantification using a NanoDrop 2000 spectrophotometer (Thermo Scientific,
561 Waltham, U.S.A.) and RNA integrity was assessed using an Agilent 2100 Bioanalyzer
562 (Agilent Technologies, Santa Clara, U.S.A.). Transcriptome sequencing and data
563 analysis were conducted by OE Biotech (Shanghai, China). The raw sequencing data
564 was submitted to the NCBI (GEO accession number: GSE286486).

565 **Transient transfection and virus infection**

566 EPC cells were transfected in 6-well and 24-well plates using transfection reagents
567 from FishTrans (MeiSenTe Biotechnology) according to the manufacturer's protocol.
568 Antiviral assays were conducted in 24-well plates by transfecting EPC cells with the
569 plasmids shown in the figure. At 24 h post-transfection, cells were infected with SVCV
570 at a multiplicity of infection (MOI = 0.001). After 24 h, supernatant aliquots were
571 harvested for detection of virus titers, the cell monolayers were fixed by 4%
572 paraformaldehyde (PFA) and stained with 1% crystal violet for visualizing CPE. For
573 virus titration, 200 μl of culture medium were collected at 48 h post-infection and used
574 for detection of virus titers according to the method of Reed and Muench. The
575 supernatants were subjected to 3-fold or 10-fold serial dilutions and then added (100 μl)
576 onto a monolayer of EPC cells cultured in a 96-well plate. After 48 or 72 h, the medium

577 was removed and the cells were washed with phosphate-buffered saline (PBS), fixed
578 by 4% PFA, and stained with 1% crystal violet. The virus titer was expressed as 50%
579 tissue culture infective dose ($TCID_{50}$/ml). For viral infection, fish were anesthetized
580 with methanesulfonate (MS-222) and intraperitoneally (i.p.) injected with 5 μl of M199
581 containing SVCV (5×10^8 $TCID_{50}$/ml). The i.p. injection of PBS was used as mock
582 infection. Then the fish were migrated into the aquarium containing new aquatic water.

583 **Luciferase activity assay**

584 EPC cells were cultured overnight in 24-well plates and subsequently co-
585 transfected with the expression plasmid and luciferase reporter plasmid. The cells were
586 infected with SVCV or transfected with poly I:C for 24 h prior to harvest. At 24 h post-
587 stimulation, cells were washed with PBS and lysed for measuring luciferase activity by
588 the Dual-Luciferase Reporter Assay System (Promega) according to the manufacturer's
589 instructions. Firefly luciferase activity was normalized based on the *Renilla* luciferase
590 activity.

591 **RNA extraction, reverse transcription, and quantitative PCR (qPCR)**

592 The RNA was extracted using TRIzol reagent (Invitrogen), and first-strand cDNA
593 was synthesized with a PrimeScript RT kit with gDNA Eraser (Takara). qPCR was
594 performed on the CFX96 Real-Time System (Bio-Rad) using SYBR green PCR Master
595 Mix (Yeasen). The PCR conditions were as follows: 95°C for 5 min and then 40 cycles
596 of 95°C for 20 s, 60°C for 20 s, and 72°C for 20 s. The primers utilized for the qPCRs
597 are presented in Table S1, and the *β-actin* gene was utilized as the internal control. The
598 relative fold changes were calculated by comparison to the corresponding controls
599 using the $2^{-\Delta\Delta Ct}$ method (where CT was the threshold cycle).

600 **Co-immunoprecipitation (Co-IP) assay**

601 EPC cells were cultured in 10-cm^2 dishes overnight and subsequently transfected
602 with 10 μg plasmid as illustrated. At 24 h post-transfection, the medium was removed
603 and cells were washed with PBS. Then the cells were lysed in 1 ml
604 radioimmunoprecipitation (RIPA) lysis buffer [1% NP-40, 50 mM Tris-HCl, pH 7.5,
605 150 mM NaCl, 1 mM EDTA, 1 mM NaF, 1 mM sodium orthovanadate (Na_3VO_4), 1
606 mM phenyl-methylsulfonyl fluoride (PMSF), 0.25% sodium deoxycholate] containing

607 protease inhibitor cocktail (Sigma-Aldrich) at 4°C for 1 h on a rocker platform. The
608 cellular debris was removed by centrifugation at 12,000 × *g* for 15 min at 4°C. The
609 supernatant was transferred to a fresh tube and incubated with 20 μl anti-Flag/HA/Myc
610 affinity gel (Sigma-Aldrich) overnight at 4°C with constant rotating incubation. These
611 samples were further analyzed by immunoblotting (IB). Immunoprecipitated proteins
612 were collected by centrifugation at 5000 × *g* for 1 min at 4°C, washed three times with
613 lysis buffer and resuspended in 50 μl 2 × SDS sample buffer. The immunoprecipitates
614 and whole cell lysates (WCLs) were analyzed by IB with the indicated antibodies (Abs).

615 ***In vivo* ubiquitination assay**

616 The transfected EPC cells were washed twice with 10 mL ice-cold PBS and
617 subsequently digested with 1 mL 0.25% trypsin-EDTA (1×) (Invitrogen) for 2-3 min
618 until the cells were dislodged. 100 μL FBS was added to neutralize the trypsin and the
619 cells were resuspended into 1.5 mL centrifuge tube, centrifuged at 2000 × *g* for 5 min.
620 The supernatant was discarded and the cell precipitations were resuspended using 1 mL
621 PBS and centrifuged at 2000 × *g* for 5 min. The collected cell precipitations were lysed
622 using 100 μL PBS containing 1% SDS and denatured by heating for 10 min. The
623 supernatants were diluted with lysis buffer until the concentration of SDS was reduced
624 to 0.1%. The diluted supernatants were incubated with 20 μL anti-Myc affinity gel
625 overnight at 4°C with constant agitation. Subsequently, these samples were subjected
626 to further analysis by IB. The immunoprecipitated proteins were collected by
627 centrifugation at 5000 × *g* for 1 min at 4°C, washed for three times with lysis buffer
628 and resuspended in 100 μL 1× SDS sample buffer.

629 **Immunoblot analysis**

630 Immunoprecipitates or WCLs were analyzed as described previously. Abs were
631 diluted as follows: anti-*β-actin* (ABclonal, AC026) at 1:10000, anti-Flag (Sigma-
632 Aldrich, F1804) at 1:3000, anti-HA (Covance, MMS-101R) at 1:3000, anti-Myc (Santa
633 Cruz Biotechnology, sc-40) at 1:3000, anti- btr32 (ABclonal, A13887) at 1:1000, anti-
634 USP8 (proteintech, 27791-1-AP) at 1:1000, and HRP-conjugated anti-mouse/rabbit
635 IgG (Thermo Scientific, 31430/31460) at 1:5000, anti-N/P/G/STING/ (prepared and
636 purified in our lab) at 1:2000.

637 **Immunofluorescence (IF)**

638 EPC cells were plated onto glass coverslips in 6-well plates and infected with
639 SVCV (MOI = 1) 24 h. The cells were then washed with PBS and fixed in 4% PFA at
640 room temperature for 1 h and permeabilized with 0.2% Triton X-100 in ice-cold PBS
641 for 15 min. The samples were incubated for 1 h at room temperature in PBS containing
642 2% bovine serum albumin (BSA, Sigma-Aldrich). After additional PBS washing, the
643 samples were incubated with anti-N Ab in PBS containing 2% BSA for 2-4 h at room
644 temperature. After three times washed by PBS, the samples were incubated with
645 secondary Ab (Goat anti-Rabbit IgG (H+L) Highly Cross-Adsorbed Secondary
646 Antibody, Alexa Fluor™ Plus 488) (Thermo Scientific, A32731, 1:5000) in PBS
647 containing 2% BSA for 1 h at room temperature. After additional PBS washing, the
648 cells were finally stained with 1 μg/ml 4′, 6-diamidino-2-phenylindole (DAPI,
649 Beyotime Institute of Biotechnology, Shanghai, China) for 10 min in the dark at room
650 temperature. Finally, the coverslips were washed and observed with a confocal
651 microscope under a 10× immersion objective (SP8; Leica).

652 **Fluorescent microscopy**

653 EPC cells were plated onto coverslips in 6-well plates and transfected with the
654 plasmids indicated for 24 h. Thereafter, the cells were washed twice with PBS and fixed
655 with 4% PFA for 1 h. After being washed three times with PBS, the cells were stained
656 with 1 μg/ml DAPI for 15 min in the dark at room temperature. Subsequently, the
657 coverslips were washed and observed with a confocal microscope under a 63× oil
658 immersion objective (SP8; Leica).

659 **Histopathology**

660 Liver and spleen tissues from three individuals of control or virus-infected fish at
661 2 days post infection (dpi) were dissected, and fixed in Bouin's Fixative overnight.
662 Subsequently, the samples were dehydrated in ascending grades of alcohol and
663 embedded into paraffin. Sections at 5 μm thickness were taken and stained with
664 hematoxylin and eosin (H&E). Histological changes were examined by optical
665 microscopy at ×40 magnification and were analyzed by the Aperio ImageScope
666 software.

Statistics analysis

For fish survival analysis, Kaplan-Meier survival curves were generated and subsequently subjected to a log-rank test. For the bar graph, one representative experiment of at least three independent experiments is shown, and each was done in triplicate. For the dot plot graph, each dot point represents one independent biological replicate. Unpaired Student's t test was used for statistical analysis. Data are presented as mean ± standard error of the mean (SEM). A p value < 0.05 was considered statistically significant.

References

1. Klein, S.L. & Huber, S. Sex Differences in Susceptibility to Viral Infection. In: Klein, S.L. & Roberts, C. (eds). *Sex Hormones and Immunity to Infection*. Springer Berlin Heidelberg: Berlin, Heidelberg, 2010, pp 93-122.

2. Klein, S.L. Sex influences immune responses to viruses, and efficacy of prophylaxis and treatments for viral diseases. *BioEssays : news and reviews in molecular, cellular and developmental biology* **34**, 1050-1059 (2012).

3. Health, G., Icrw, Aphrc & Gautam, A. *The-COVID-19-Sex-Disaggregated-Data-Tracker-Update*, 2020.

4. Guha-Sapir, D. & Schimmer, B. Dengue fever: new paradigms for a changing epidemiology. *Emerg Themes Epidemiol* **2**, 1 (2005).

5. Tsay, P.K. *et al.* Impact of gender, viral transmission and aging in the prevalence of hepatitis B surface antigen. *Chang Gung medical journal* **32**, 155-164 (2009).

6. Burguete-García, A.I. *et al.* Hepatitis C seroprevalence and correlation between viral load and viral genotype among primary care clients in Mexico. *Salud publica de Mexico* **53 Suppl 1**, S7-12 (2011).

7. Liva, S.M. & Voskuhl, R.R. Testosterone acts directly on $CD4^+$T lymphocytes to increase IL-10 production. *Journal of immunology* **167**, 2060-2067 (2001).

8. Pinheiro, I., Dejager, L. & Libert, C. X-chromosome-located microRNAs in immunity: might they explain male/female differences? The X chromosome-genomic context may affect X-located miRNAs and downstream signaling, thereby contributing to the enhanced immune response of females.

BioEssays : news and reviews in molecular, cellular and developmental biology **33**, 791-802 (2011).

9. Sharma, S. & Eghbali, M. Influence of sex differences on microRNA gene regulation in disease. *Biology of sex differences* **5**, 3 (2014).

10. Akira, S., Uematsu, S. & Takeuchi, O. Pathogen recognition and innate immunity. *Cell* **124**, 783-801 (2006).

11. Chen, S.N., Zou, P.F. & Nie, P. Retinoic acid-inducible gene I (RIG-I)-like receptors (RLRs) in fish: current knowledge and future perspectives. *Immunology* **151**, 16-25 (2017).

12. Ishikawa, H. & Barber, G.N. STING is an endoplasmic reticulum adaptor that facilitates innate immune signalling. *Nature* **455**, 674-678 (2008).

13. Ni, G.X., Ma, Z. & Damania, B. cGAS and STING: At the intersection of DNA and RNA virus-sensing networks. *PLoS pathogens* **14** (2018).

14. Aguirre, S. *et al.* DENV Inhibits Type I IFN Production in Infected Cells by Cleaving Human STING. *PLoS pathogens* **8** (2012).

15. Nazmi, A., Mukhopadhyay, R., Dutta, K. & Basu, A. STING Mediates Neuronal Innate Immune Response Following Japanese Encephalitis Virus Infection. *Scientific reports* **2** (2012).

16. You, F.P. *et al.* ELF4 is critical for induction of type I interferon and the host antiviral response. *Nature immunology* **14**, 1237-+ (2013).

17. Lau, L., Gray, E.E., Brunette, R.L. & Stetson, D.B. DNA tumor virus oncogenes antagonize the cGAS-STING DNA-sensing pathway. *Science* **350**, 568-571 (2015).

18. Kim, Y.M. *et al.* A review of the literature on common CYP17A1 mutations in adults with 17-hydroxylase/17,20-lyase deficiency, a case series of such mutations among Koreans and functional characteristics of a novel mutation. *Metabolism* **63**, 42-49 (2014).

19. Zhou, L.Y. *et al.* A novel type of P450c17 lacking the lyase activity is responsible for C21-steroid biosynthesis in the fish ovary and head kidney. *Endocrinology* **148**, 4282-4291 (2007).

20. Shi, S.C. *et al.* Characterization of the Interrenal Gland and Sexual Traits Development in *cyp17a2*-Deficient Zebrafish. *Front Endocrinol* **13** (2022).

21. Matsuda, M. *et al.* DMY is a Y-specific DM-domain gene required for male development in the medaka fish. *Nature* **417**, 559-563 (2002).

22. Yoshida, K. *et al.* B Chromosomes Have a Functional Effect on Female Sex Determination in Lake Victoria Cichlid Fishes. *Plos Genet* **7** (2011).

23. Hayashi, Y. *et al.* High Temperature Causes Masculinization of Genetically Female Medaka by Elevation of Cortisol. *Mol Reprod Dev* **77**, 679-686 (2010).

24. Zajitschek, S.R. *et al.* Sexual dimorphism in trait variability and its eco-evolutionary and statistical implications. *Elife* **9** (2020).

25. Gan, E.S., Ting, D.H.R. & Chan, K.R. The mechanistic role of antibodies to dengue virus in protection and disease pathogenesis. *Expert Rev Anti-Infe* **15**, 111-119 (2017).

26. Wald, A. Herpes Simplex Virus Type 2 Transmission: Risk Factors and Virus Shedding. *Herpes : the journal of the IHMF* **11 Suppl 3**, 130A-137A (2004).

27. Klein, S.L. & Flanagan, K.L. Sex differences in immune responses. *Nature Reviews Immunology* **16**, 626-638 (2016).

28. Vial, P.A. *et al.* Hantavirus in humans: a review of clinical aspects and management. *Lancet Infect Dis* **23**, E371-E382 (2023).

29. Eshima, N. *et al.* Sex- and Age-Related Differences in Morbidity Rates of 2009 Pandemic Influenza A H1N1 Virus of Swine Origin in Japan. *PloS one* **6** (2011).

30. Cui, J., Shen, Y. & Li, R. Estrogen synthesis and signaling pathways during aging: from periphery to brain. *Trends Mol Med* **19**, 197-209 (2013).

31. Lu, L.F. *et al.* Fish female-biased gene leads to female antiviral response attenuation between sexes by autophagic degradation of MITA. *PLoS pathogens* **18** (2022).

32. Gui, J.-F., Zhou, L. & Li, X.-y. Rethinking fish biology and biotechnologies in the challenge era for burgeoning genome resources and strengthening food security. *Water Biology and Security* **1** (2021).

33. Woznica, A. *et al.* STING mediates immune responses in the closest living relatives of animals. *Elife* **10** (2021).

34. Ran, Y., Shu, H.B. & Wang, Y.Y. MITA/STING: a central and multifaceted mediator in innate immune response. *Cytokine Growth F R* **25**, 631-639 (2014).

35. Biacchesi, S., Merour, E., Lamoureux, A., Bernard, J. & Bremont, M. Both STING and MAVS fish orthologs contribute to the induction of interferon mediated by RIG-I. *PloS one* **7**, e47737 (2012).

36. Lu, L.-F. *et al.* Fish herpesvirus KLP manipulates Beclin1 to selectively degrade MITA through a precise autophagic manner for immune evasion. *Water Biology and Security* **2**, 100092 (2023).

37. Li, S., Lu, L.-F. & Zhang, C. The LxIS motif is the language between virus and host RLRs: From fish to mammalian viruses. *Water Biology and Security* **3**, 100246 (2024).

38. Effner, R. *et al.* Cytochrome P450s in human immune cells regulate IL-22 and c-Kit via an AHR feedback loop. *Scientific reports* **7** (2017).

39. Chu, P.F. *et al.* Identification, expression and functional characterisation of in grass carp (Ctenopharyngodon idella). *Fish Shellfish Immun* **95**, 35-43 (2019).

Figure legends

Figure 1. Male fish show stronger viral resistance than females.

(A) Survival (Kaplan-Meier Curve) of male and female zebrafish (n = 15 per group) at various days after i.p. injected with SVCV (5×10^8 $TCID_{50}$/ml, 5 μL/individual). (B) Sex-specific morphological alterations in zebrafish given i.p. injection of SVCV for 48 h (n = 3 per group). (C) Microscopy of H&E-stained liver and spleen sections from male and female zebrafish treated with SVCV for 48 h. (D) IF analysis of SVCV-N protein in liver and spleen of male and female zebrafish treated with SVCV for 48 h. (E) qPCR analysis of *svcv-n* mRNA in the liver and spleen of male and female zebrafish (n = 26 per group) given i.p. injection of SVCV for 48 h. (F) IB analysis of SVCV proteins in the liver and spleen sections of male and female zebrafish (n = 7 per group) treated with SVCV for 48 h. (G) The viral titer of heart in male and female zebrafish (n

812 = 40 per group) treated with SVCV for 48 h.

813

814 **Figure 2. Male-biased cyp17a2 regulates RLR-mediated antiviral immunity.**

815 (A) The differently expressed gene number of mRNA variations presented as a volcano
816 plot in head-kidney of male and female zebrafish. (B) Heatmap view of mRNA
817 variations of eight sex-regulated genes in the head-kidney of male and female zebrafish.
818 Values are represented as $\log_2^{(FPKM+1)}$. (C) Heatmap view of *cyp17a2* mRNA in the brain,
819 heart, head-kidney, gill, liver, spleen, body-kidney, gonad, gut, muscle, and skin of male
820 and female zebrafish (n = 5 per group). Expression values [$\log_2^{(fold\ change)}$] were
821 transformed to Z-scores across rows for each gene to highlight patterns of relative
822 expression. (D) IB analysis of Cyp17a2 in the heart, head-kidney, gill, liver, spleen,
823 body-kidney, gonad, and skin of male and female zebrafish (n = 5 per group). (E)
824 Survival (Kaplan-Meier Curve) of *cyp17a2*$^{+/+}$ and *cyp17a2*$^{-/-}$ male zebrafish (n = 16 per
825 group) at various days after i.p. injected with SVCV (5 × 10^8 TCID50/ml, 5
826 μl/individual). (F) qPCR analysis of *svcv-n* mRNA in the liver and spleen of *cyp17a2*$^{+/+}$
827 and *cyp17a2*$^{-/-}$ male zebrafish (n = 20 per group) given i.p. injection of SVCV for 48 h.
828 (G) qPCR analysis of *ifnφ1* mRNA in the liver and spleen of *cyp17a2*$^{+/+}$ and *cyp17a2*$^{-/-}$
829 male zebrafish (n = 20 per group) given i.p. injection of SVCV for 48 h.

830

831 **Figure 3. Cyp17a2 upregulates IFN expression and inhibits viral replication.**

832 (A and E) Luciferase activity of IFNφ1pro in EPC cells transfected with indicated
833 plasmids for 24 h, and then untreated or transfected with poly I:C (0.5 μg) or infected
834 with SVCV (MOI = 1) for 24 h before luciferase assays. (B) qPCR analysis of *cyp17a2*
835 in EPC cells transfected with indicated plasmids for 24 h, and then untreated or
836 transfected with poly I:C (2 μg) or infected with SVCV (MOI = 1) for 24 h. (C and D)
837 IB analysis of proteins in EPC cells transfected with indicated plasmids for 24 h. (F)
838 Heatmap view of mRNA variations of SVCV-activated ISG sets in the Cyp17a2-
839 overexpressing cells or *cyp17a2* knockdown cells and infected with SVCV for 24 h.
840 Expression values are $\log_2^{(FPKM+1)}$ transformed and presented as row Z-scores. (G)
841 qPCR analysis of *ifn* in EPC cells transfected with indicated plasmids for 24 h, and then

842 untreated or infected with SVCV (MOI = 1) for 24 h. (H) Plaque assay of virus titers in
843 EPC cells or GICB cells transfected with indicated plasmids for 24 h, followed by
844 SVCV or CyHV-2 challenge for 24 h or 48 h. (I and J) qPCR and IB analysis of SVCV
845 genes in EPC cells transfected with indicated plasmids for 24 h, followed by SVCV
846 challenge for 24 h. (K) IF analysis of SVCV proteins in EPC cells transfected with
847 indicated plasmids for 24 h, followed by SVCV challenge for 24 h.
848
849 **Figure 4. Cyp17a2 physically interacts with STING and stabilizes its expression.**
850 (A-C and E) IB analysis of WCLs and proteins immunoprecipitated with anti- Flag or
851 HA Ab-conjugated agarose beads from EPC cells transfected with indicated plasmids
852 for 24 h. (D) Schematic representation of full-length STING and its mutants. (F and G)
853 Confocal microscopy of Cyp17a2 and ER or STING and its mutants in EPC cells
854 transfected with indicated plasmids for 24 h. The coefficient of colocalization was
855 determined by qualitative analysis of the fluorescence intensity of the selected area in
856 Merge. (H) qPCR analysis of *sting* in EPC cells transfected with indicated plasmids for
857 24 h, followed by untreated or infected with SVCV (MOI = 1) for 24 h. (I) IB analysis
858 of proteins in EPC cells transfected with indicated plasmids for 24 h. (J) IB analysis of
859 proteins in EPC cells transfected with indicated plasmids for 24 h, followed by
860 untreated or infected with SVCV (MOI = 1) for 24 h. (K) IB analysis of proteins in EPC
861 cells transfected with indicated plasmids for 18 h, then treated with CHX for 4 h and 8
862 h.
863
864 **Figure 5. Cyp17a2 potentiates STING-induced IFN production and antiviral**
865 **responses.**
866 (A and B) Luciferase activity of IFNφ1pro in EPC cells transfected with indicated
867 plasmids for 24 h before luciferase assays. (C and D) qPCR analysis of *ifn* in EPC cells
868 transfected with indicated plasmids for 24 h. (E and H) Detection of virus titers in EPC
869 cells transfected with indicated plasmids for 24 h and then infected with SVCV (MOI
870 = 1) for 24 h. (F and J) IB analysis of proteins in EPC cells transfected with indicated
871 plasmids for 24 h and then untreated or infected with SVCV (MOI = 1) for 24 h. (G and

872 I) qPCR analysis of SVCV genes in EPC cells transfected with indicated plasmids for
873 24 h, followed by SVCV challenge for 24 h.
874
875 **Figure 6. Cyp17a2 stabilizes STING by orchestrating btr32-catalyzed K33-linked**
876 **polyubiquitination.**
877 (A) IB analysis of proteins in EPC cells transfected with indicated plasmids for 18 h,
878 then treated with CHX and DMSO, MG132, or CQ for 4 h and 8 h. (B and C) STING
879 ubiquitination assays in EPC cells transfected with indicated plasmids for 24 h. (D-G,
880 K) IB analysis of WCLs and proteins immunoprecipitated with anti-Flag Ab-conjugated
881 agarose beads from EPC cells transfected with indicated plasmids for 24 h. (H and I)
882 Confocal microscopy of btr32 and ER or STING or Cyp17a2 in EPC cells transfected
883 with indicated plasmids for 24 h. The coefficient of colocalization was determined by
884 qualitative analysis of the fluorescence intensity of the selected area in Merge. (J)
885 Colocalization analyses of figure 6I were performed by calculating Pearson correlation
886 coefficient. (L and M) Luciferase activity of IFNφ1pro and qPCR analysis of *vig1* in
887 EPC cells transfected with indicated plasmids for 24 h. (N) IB analysis of proteins in
888 EPC cells transfected with indicated plasmids for 24 h.
889
890 **Figure 7 Cyp17a2-mediated ubiquitination of STING is dependent on the K203.**
891 (A and B, G and H, and M) STING ubiquitination assays in EPC cells transfected with
892 indicated plasmids for 24 h. (C) Mass spectrometry analysis of a peptide derived from
893 ubiquitinated STING-Myc. (D) IB analysis of proteins in EPC cells transfected with
894 indicated plasmids for 24 h. (E and F) Luciferase activity of IFNφ1pro and qPCR
895 analysis of *ifn* in EPC cells transfected with indicated plasmids for 24 h. (I) Schematic
896 representation of full-length btr32 and its mutants. (J-L) IB of WCLs and proteins
897 immunoprecipitated with anti-Flag/HA Ab-conjugated agarose beads from EPC cells
898 transfected with indicated plasmids for 24 h.
899
900 **Figure 8 Cyp17a2 induces proteasomal degradation of the SVCV P protein by**
901 **catalyzing K33-linked polyubiquitination.**

902 (A-C) IB analysis of WCLs and proteins immunoprecipitated with anti-Flag, anti-HA,
903 or anti-Myc Ab-conjugated agarose beads from EPC cells transfected with indicated
904 plasmids for 24 h. (D) IB analysis of proteins in EPC cells transfected with indicated
905 plasmids for 24 h. (E) Fluorescent analysis of proteins in EPC cells transfected with
906 indicated plasmids for 24 h. (F) Confocal microscopy of P and Cyp17a2 in EPC cells
907 transfected with indicated plasmids for 24 h. The coefficient of colocalization was
908 determined by qualitative analysis of the fluorescence intensity of the selected area in
909 Merge. (G) IB analysis of proteins in EPC cells transfected with indicated plasmids for
910 18 h, followed by treatments of MG132 (10 μM), 3-MA (2 mM), Baf-A1 (100 nM),
911 and CQ (50 μM) for 6 h, respectively. (H-K) P protein ubiquitination assays in EPC
912 cells transfected with indicated plasmids for 18 h, followed by MG132 treatments for
913 6 h.
914
915 **Figure 9 Cyp17a2 targets the K12 site of the P protein for K33-linked**
916 **polyubiquitination.**
917 (A) List of proteins interacting with P protein detected by mass spectrometry. (B and C,
918 E, O) IB analysis of WCLs and proteins immunoprecipitated with anti-HA/Myc Ab-
919 conjugated agarose beads from EPC cells transfected with indicated plasmids for 24 h.
920 (D) Confocal microscopy of USP8 and Cyp17a2 or P protein in EPC cells transfected
921 with indicated plasmids for 24 h. The coefficient of colocalization was determined by
922 qualitative analysis of the fluorescence intensity of the selected area in Merge. (F and
923 G, K) IB analysis of proteins in EPC cells transfected with indicated plasmids for 24 h.
924 (H and I, L and M, P) P protein ubiquitination assays in EPC cells transfected with
925 indicated plasmids for 18 h, followed by MG132 treatments for 6 h. (J) Mass
926 spectrometry analysis of a peptide derived from ubiquitinated P-Myc. (N) Schematic
927 representation of full-length USP8 and its mutants.
928
929 **Figure 10 A mechanistic model illustrating the dual regulatory roles of Cyp17a2**
930 **in upregulating STING expression and degrading SVCV P protein.**
931 Upon virus infection, male-biased autosomal gene *cyp17a2* enhances antiviral

932 responses in males. Mechanistically, Cyp17a2, an ER-localized protein, stabilizes
933 STING expression through recruitment of the E3 ubiquitin ligase btr32, promoting
934 K33-linked polyubiquitination. Furthermore, Cyp17a2 facilitates proteasomal
935 degradation of the SVCV P protein by engaging USP8 to reduce its K33-linked
936 polyubiquitination, thereby amplifying antiviral IFN responses.
937
938 **Figure S1 The male-biased expression of Cyp17a2 governs RLR antiviral signaling.**
939 (A) qPCR analysis of *cyp17a2* mRNA in the head-kidney of male and female zebrafish
940 (n = 50 per group). (B) qPCR analysis of *cyp17a2* mRNA in the ZF4 or EPC cells
941 infected with SVCV for the indicated times. (C) IB analysis of Cyp17a2 in ZF4 and
942 EPC cells infected with SVCV for the indicated times. (D) Microscopy of H&E-stained
943 liver and spleen sections from *cyp17a2*$^{+/+}$ and *cyp17a2*$^{-/-}$ male zebrafish treated with
944 SVCV for 48 h. (E) IF analysis of SVCV-N protein in the liver and spleen of *cyp17a2*$^{+/+}$
945 and *cyp17a2*$^{-/-}$ male zebrafish treated with SVCV for 48 h. (F) The viral titer of heart in
946 *cyp17a2*$^{+/+}$ and *cyp17a2*$^{-/-}$ male zebrafish (n = 15 per group) treated with SVCV for 48
947 h. (G) IB analysis of SVCV proteins in the liver and spleen sections of *cyp17a2*$^{+/+}$ and
948 *cyp17a2*$^{-/-}$ male zebrafish (n = 3 per group) treated with SVCV for 48 h. (H) The
949 differently expressed gene number of mRNA variations in liver of *cyp17a2*$^{+/+}$ and
950 *cyp17a2*$^{-/-}$ male zebrafish infected with SVCV. (I) KEGG pathway enrichment map
951 showing the top 10 signaling pathways of total. (J) GSEA of differentially expressed
952 genes in the liver of *cyp17a2*$^{+/+}$ and *cyp17a2*$^{-/-}$male zebrafish infected with SVCV and
953 enrichment of RLR signaling pathway. The *p*-values were corrected for the False
954 Discovery Rate (FDR) method, and modules with *p*-values less than 0.05 were selected
955 as significant.
956
957 **Figure S2 Heatmap view of mRNA variations of RLR-mediated ISGs sets in the**
958 **liver of *cyp17a2*$^{+/+}$ and *cyp17a2*$^{-/-}$ male zebrafish infected with SVCV.** Expression
959 values are $\log_2^{(FPKM+1)}$ transformed and presented as row Z-scores.
960
961 **Figure S3 Cyp17a2 enhances IFN production to inhibit viral replication.** (A-D)

962 Luciferase activity of IFNφ3pro and ISRE in EPC cells transfected with indicated
963 plasmids for 24 h, and then untreated or transfected with poly I:C (0.5 μg) or infected
964 with SVCV (MOI = 1) for 24 h before luciferase assays. (E) qPCR analysis of *vig1* in
965 EPC cells transfected with indicated plasmids for 24 h, and then untreated or infected
966 with SVCV (MOI = 1) for 24 h. (F) Plaque assay of virus titers in EPC cells or GICB
967 cells transfected with indicated plasmids for 24 h, followed by SVCV or CyHV-2
968 challenge for 24 h or 48 h. (G and H) qPCR and IB analysis of SVCV genes in EPC
969 cells transfected with indicated plasmids for 24 h, followed by SVCV challenge for 24
970 h. (I) IF analysis of SVCV proteins in EPC cells transfected with indicated plasmids for
971 24 h, followed by SVCV challenge for 24 h.
972
973 **Figure S4 STING stability is enhanced by Cyp17a2.** (A) Colocalization analyses of
974 figure 4G were performed by calculating Pearson correlation coefficient. (B)
975 Fluorescent analysis of proteins in EPC cells transfected with indicated plasmids for 24
976 h. The fluorescence intensity (arbitrary unit, a.u.) was recorded by the LAS X software,
977 and the data were expressed as mean ± SD, n = 5. (C) IB analysis of proteins in EPC
978 cells transfected with indicated plasmids for 24 h, followed by untreated or transfected
979 with poly I:C (2 μg) for 24 h. (D and E) IB analysis of proteins in EPC cells transfected
980 with indicated plasmids for 18 h, then treated with CHX for 4 h and 8 h.
981
982 **Figure S5 Cyp17a2 enhances STING-mediated IFN activation and antiviral**
983 **defense.** (A and B) Luciferase activity of ISRE in EPC cells transfected with indicated
984 plasmids for 24 h before luciferase assays. (C and D) qPCR analysis of *vig1* in EPC
985 cells transfected with indicated plasmids for 24 h. (E and H) Plaque assay in EPC cells
986 transfected with indicated plasmids for 24 h and then infected with SVCV (MOI = 1)
987 for 24 h. (F and I) IF analysis of N protein and P protein in EPC cells transfected with
988 indicated plasmids for 24 h, followed by SVCV challenge for 24 h. The fluorescence
989 intensity (arbitrary unit, a.u.) was recorded by the LAS X software, and the data were
990 expressed as mean ± SD, n = 5. (G) IB analysis of proteins in EPC cells transfected
991 with indicated plasmids for 24 h.

Figure S6 Cyp17a2 promotes STING stabilization by facilitating btr32-catalyzed K33-linked polyubiquitination. (A) STING ubiquitination assays in EPC cells transfected with indicated plasmids for 24 h. (B) IB analysis of WCLs and proteins immunoprecipitated with anti-Flag Ab-conjugated agarose beads from EPC cells transfected with indicated plasmids for 24 h. (C and D, G) IB analysis of proteins in EPC cells transfected with indicated plasmids for 24 h. (E and F) Luciferase activity of IFNφ1pro and qPCR analysis of *vig1* in EPC cells transfected with indicated plasmids for 24 h.

Figure S7 The K203 residue is essential for the ubiquitination of STING mediated by Cyp17a2. (A-E) STING ubiquitination assays in EPC cells transfected with indicated plasmids for 24 h.

Figure S8 Cyp17a2 mediates K33-linked polyubiquitination of the P protein at K12. (A and C) IB analysis of WCLs and proteins immunoprecipitated with anti-Flag/Myc Ab-conjugated agarose beads from EPC cells transfected with indicated plasmids for 24 h. (B) Colocalization analyses of figure 9D were performed by calculating Pearson correlation coefficient. (D) IB analysis of proteins in EPC cells transfected with indicated plasmids for 24 h. (E-I) P protein ubiquitination assays in EPC cells transfected with indicated plasmids for 18 h, followed by MG132 treatments for 6 h.

Table S1 List of primer sequences used in this study.

Table S2 List of all identified genes in FHK-vs-MHK in transcriptomic analysis.

Table S3 Heatmap view of mRNA variations of SVCV-activated ISG sets in the Cyp17a2-overexpressing cells or *cyp17a2* knockdown cells.

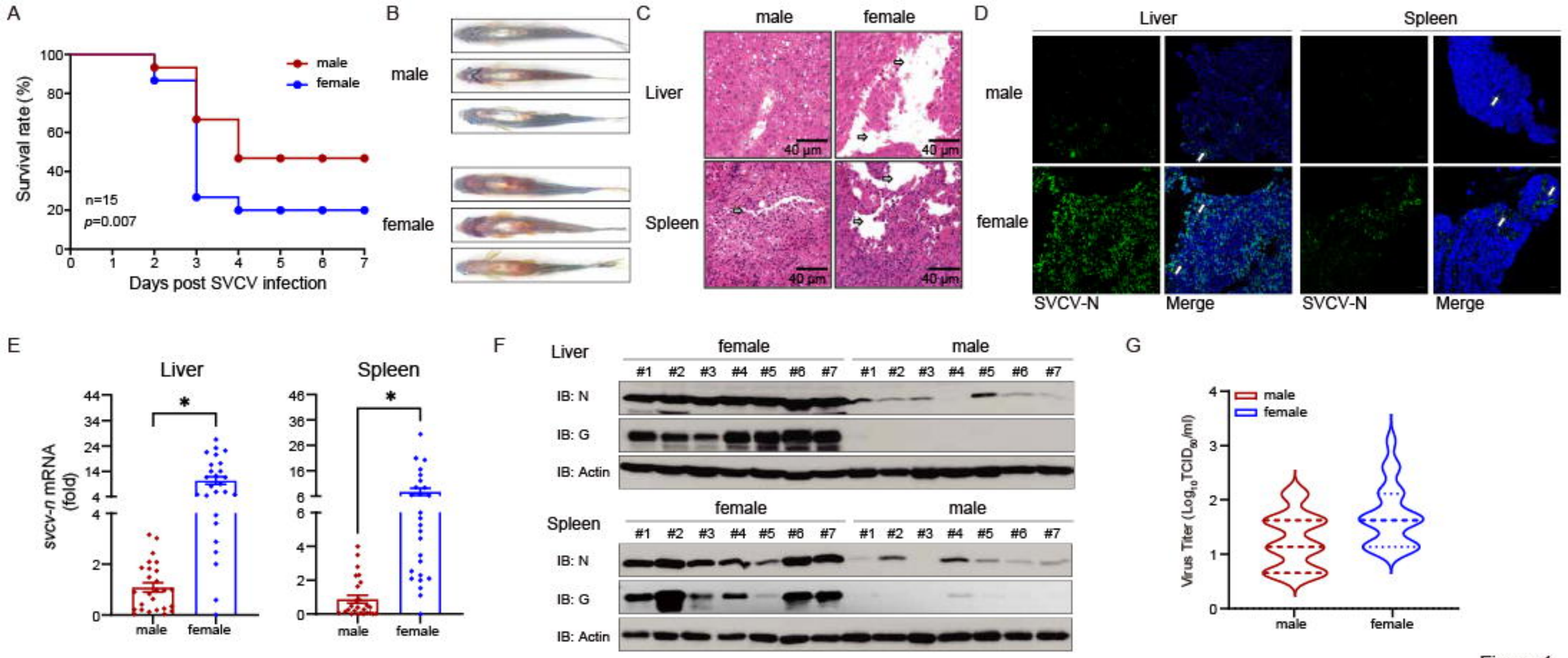
A
Survival rate (%)
Days post SVCV infection
male
female
n=15
p=0.007
B
male
female
C
male
female
Liver
Spleen
40 μm
D
Liver
Spleen
male
female
SVCV-N
Merge
E
Liver
Spleen
svcv-n mRNA (fold)
male
female
F
Liver
Spleen
female
male
IB: N
IB: G
IB: Actin
G
Virus Titer (Log10TCID50/ml)
male
female

Figure 1

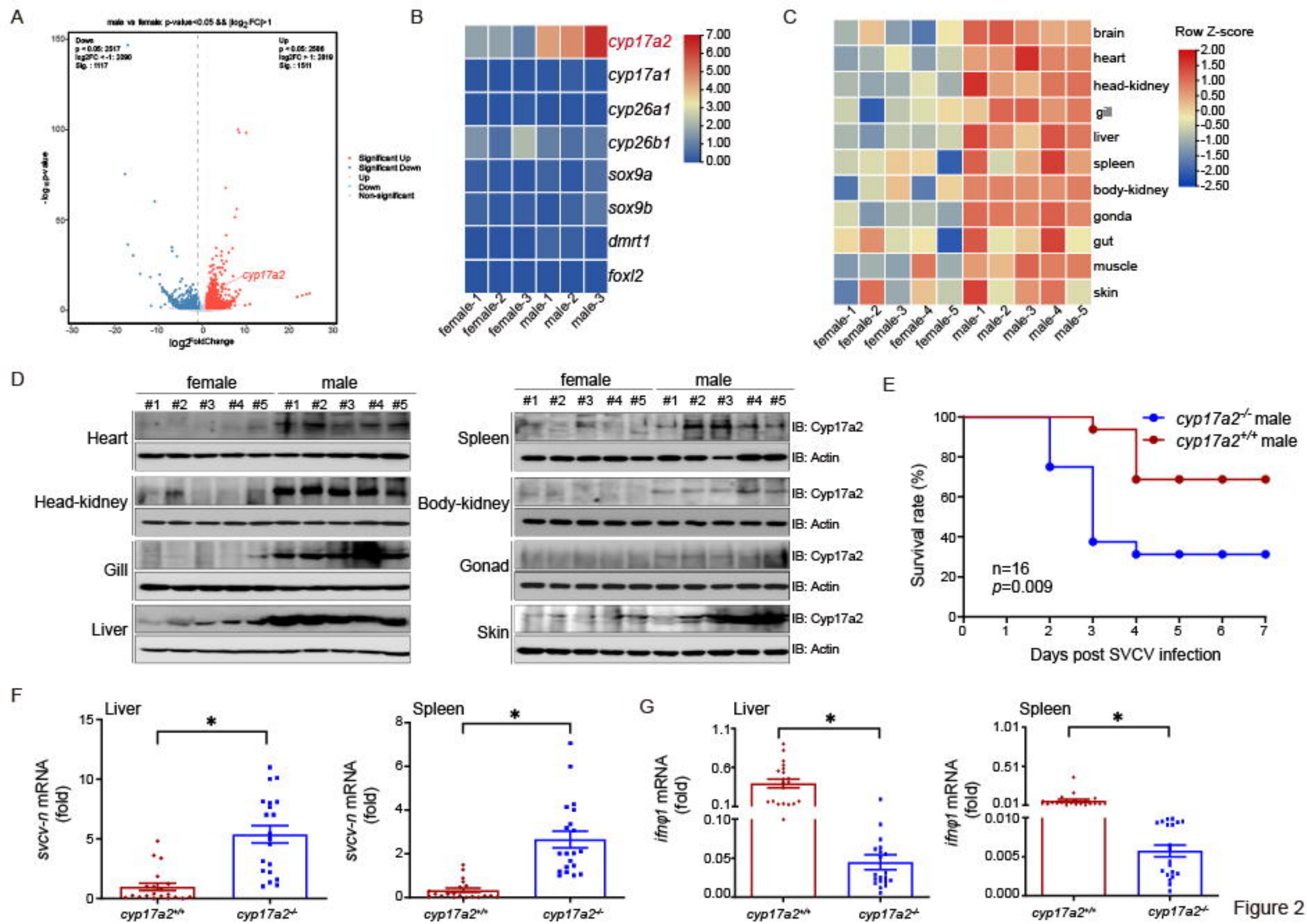
A
male vs female: p-value<0.05 && |log2FC|>1
Down
Up
Significant Up
Significant Down
Up
Down
Non-significant
cyp17a2
-log10pvalue
log2FoldChange
B
cyp17a2
cyp17a1
cyp26a1
cyp26b1
sox9a
sox9b
dmrt1
foxl2
female-1
female-2
female-3
male-1
male-2
male-3
C
Row Z-score
brain
heart
head-kidney
gill
liver
spleen
body-kidney
gonda
gut
muscle
skin
female-1
female-2
female-3
female-4
female-5
male-1
male-2
male-3
male-4
male-5
D
female
male
#1 #2 #3 #4 #5
Heart
Head-kidney
Gill
Liver
Spleen
Body-kidney
Gonad
Skin
IB: Cyp17a2
IB: Actin
E
cyp17a2-/- male
cyp17a2+/+ male
Survival rate (%)
n=16
p=0.009
Days post SVCV infection
F
Liver
Spleen
svcv-n mRNA (fold)
cyp17a2+/+
cyp17a2-/-
G
ifnφ1 mRNA (fold)

Figure 2

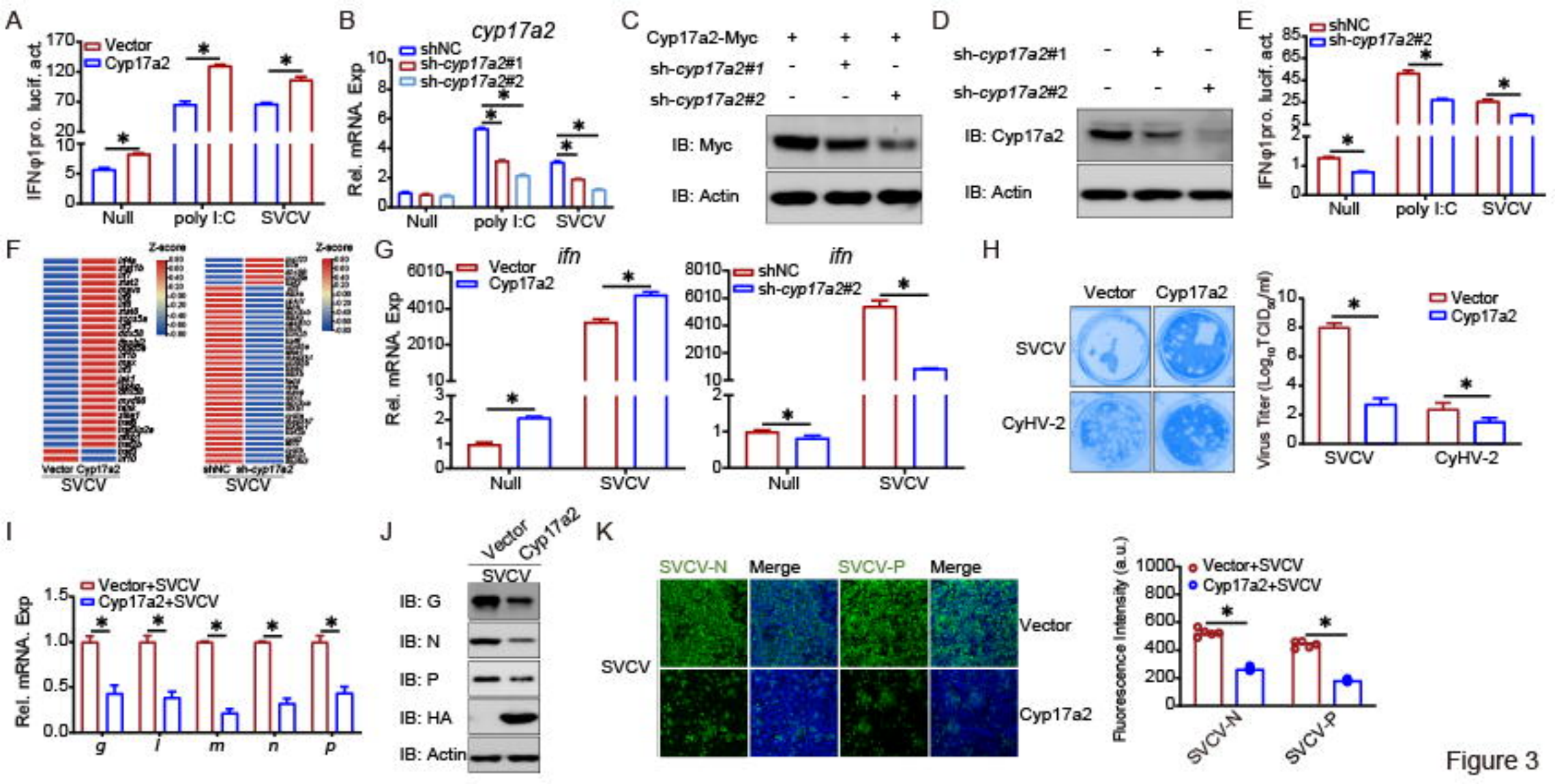
A
Vector
Cyp17a2
IFNφ1pro. lucif. act.
Null
poly I:C
SVCV
B
cyp17a2
shNC
sh-cyp17a2#1
sh-cyp17a2#2
Rel. mRNA. Exp
C
Cyp17a2-Myc
sh-cyp17a2#1
sh-cyp17a2#2
IB: Myc
IB: Actin
D
sh-cyp17a2#1
sh-cyp17a2#2
IB: Cyp17a2
IB: Actin
E
shNC
sh-cyp17a2#2
F
Z-score
Vector Cyp17a2
shNC sh-cyp17a2
SVCV
G
ifn
Vector
Cyp17a2
shNC
sh-cyp17a2#2
Rel. mRNA. Exp
H
Vector
Cyp17a2
SVCV
CyHV-2
Virus Titer (Log10TCID50/ml)
I
Vector+SVCV
Cyp17a2+SVCV
Rel. mRNA. Exp
g
l
m
n
p
J
Vector
Cyp17a2
SVCV
IB: G
IB: N
IB: P
IB: HA
IB: Actin
K
SVCV-N
Merge
SVCV-P
Merge
SVCV
Vector
Cyp17a2
Fluorescence Intensity (a.u.)
Vector+SVCV
Cyp17a2+SVCV
SVCV-N
SVCV-P

Figure 3

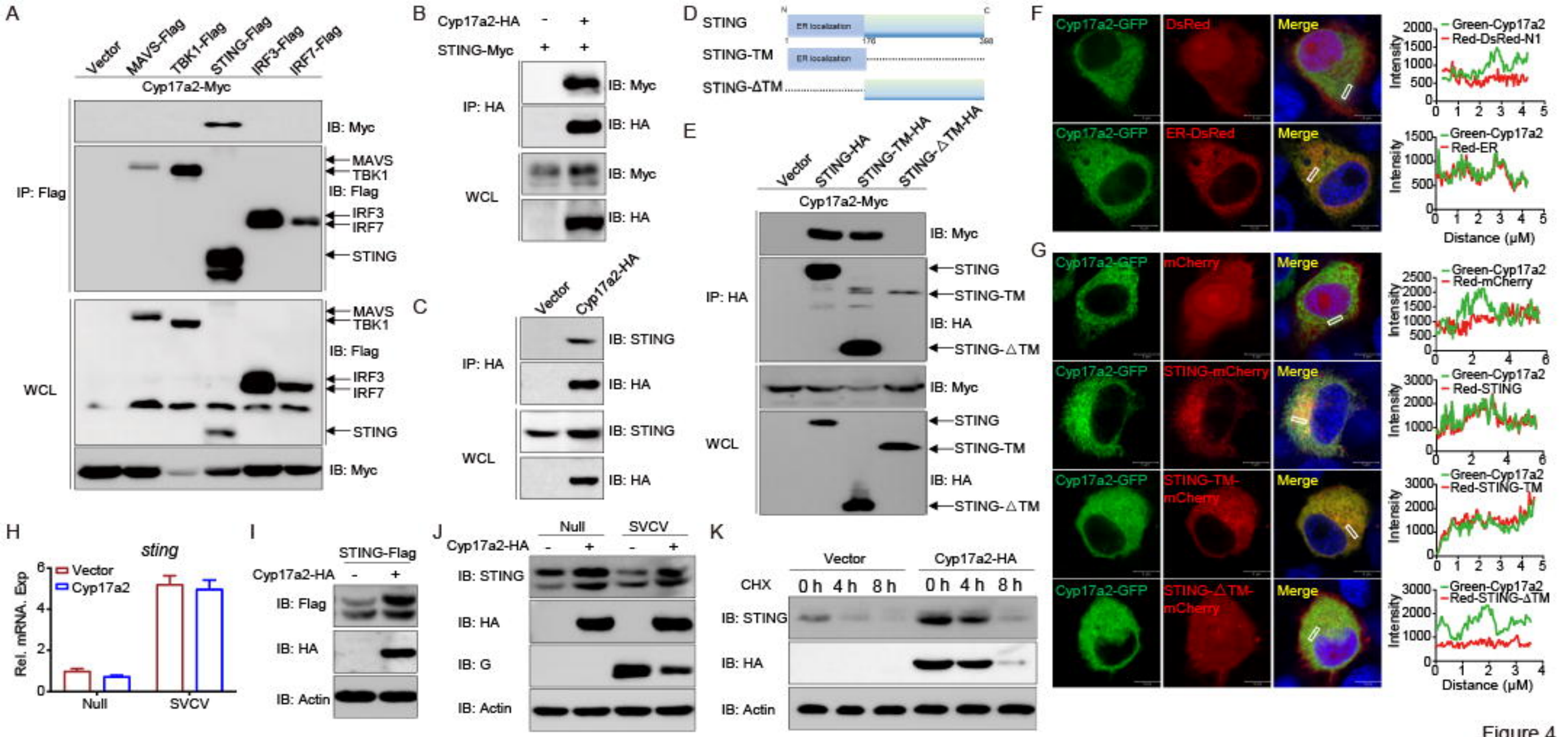
A
Vector
MAVS-Flag
TBK1-Flag
STING-Flag
IRF3-Flag
IRF7-Flag
Cyp17a2-Myc
IP: Flag
IB: Myc
MAVS
TBK1
IB: Flag
IRF3
IRF7
STING
WCL
IB: Myc
B
Cyp17a2-HA
STING-Myc
IP: HA
IB: Myc
IB: HA
WCL
C
Vector
Cyp17a2-HA
IB: STING
D
STING
STING-TM
STING-ΔTM
ER localization
E
STING-HA
STING-TM-HA
STING-ΔTM-HA
F
Cyp17a2-GFP
DsRed
ER-DsRed
Merge
Green-Cyp17a2
Red-DsRed-N1
Red-ER
Intensity
Distance (μM)
G
mCherry
STING-mCherry
STING-TM-mCherry
STING-ΔTM-mCherry
Red-mCherry
Red-STING
Red-STING-TM
Red-STING-ΔTM
H
sting
Vector
Cyp17a2
Rel. mRNA. Exp
Null
SVCV
I
STING-Flag
IB: Flag
IB: Actin
J
IB: G
K
CHX
0 h
4 h
8 h

Figure 4

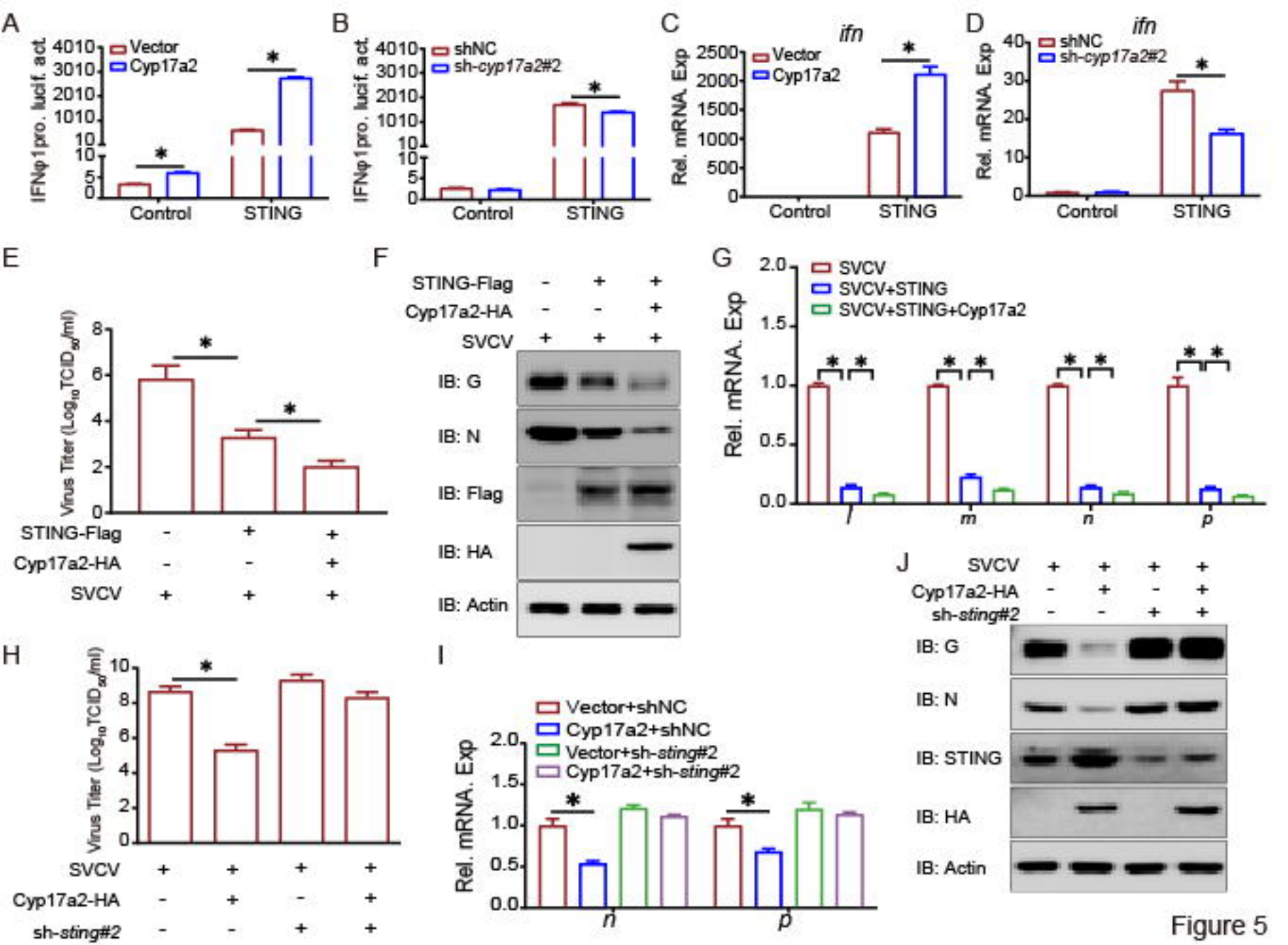
A
IFNφ1pro. lucif. act.
Vector
Cyp17a2
Control
STING
B
shNC
sh-cyp17a2#2
C
ifn
Rel. mRNA. Exp
D
E
Virus Titer (Log10TCID50/ml)
STING-Flag
Cyp17a2-HA
SVCV
F
IB: G
IB: N
IB: Flag
IB: HA
IB: Actin
G
SVCV
SVCV+STING
SVCV+STING+Cyp17a2
l
m
n
p
H
I
Vector+shNC
Cyp17a2+shNC
Vector+sh-sting#2
Cyp17a2+sh-sting#2
J
sh-sting#2
IB: STING

Figure 5

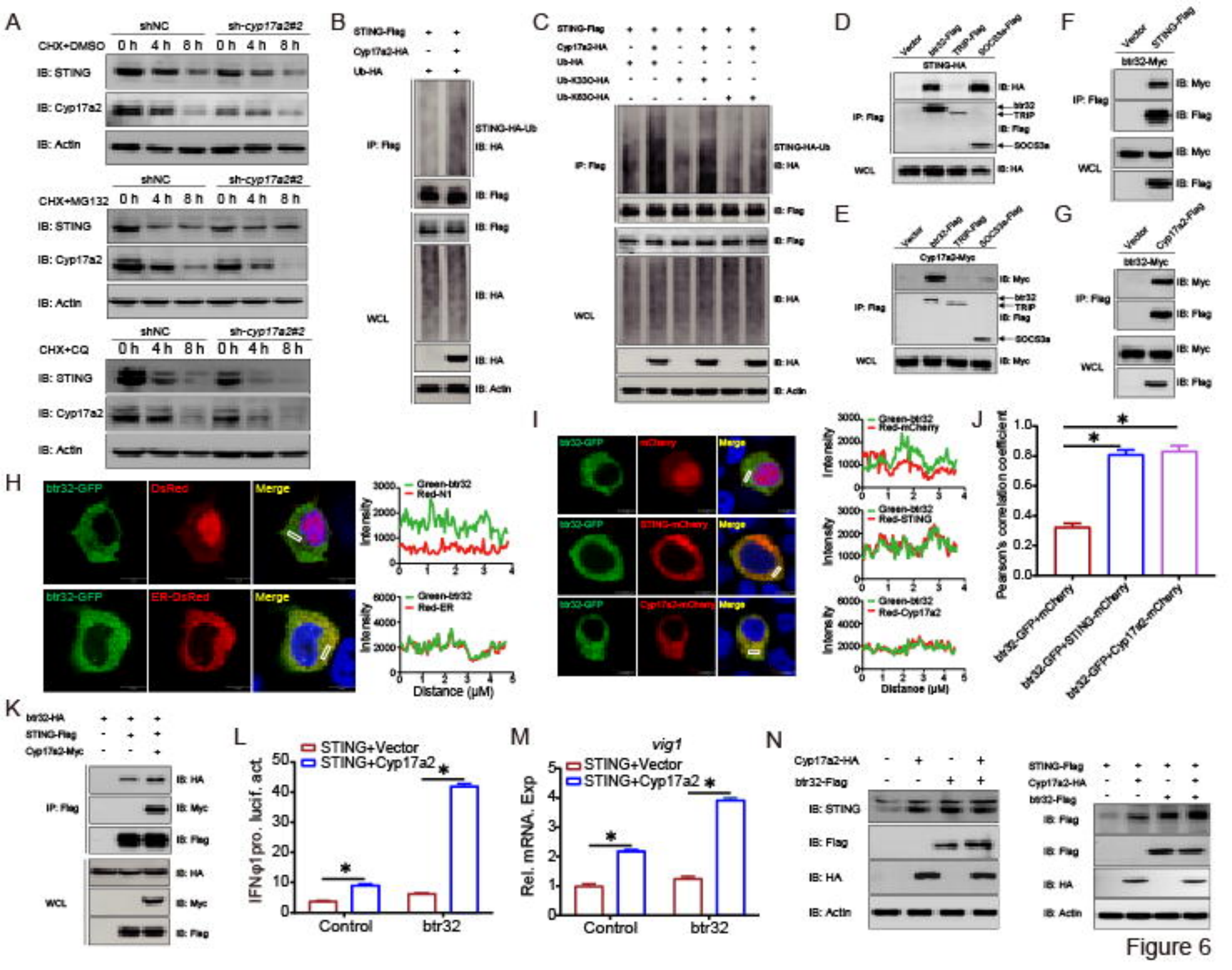
A
shNC
sh-cyp17a2#2
CHX+DMSO
0 h 4 h 8 h 0 h 4 h 8 h
IB: STING
IB: Cyp17a2
IB: Actin
CHX+MG132
CHX+CQ
B
STING-Flag
Cyp17a2-HA
Ub-HA
IP: Flag
STING-HA-Ub
IB: HA
IB: Flag
WCL
IB: Actin
C
Ub-K33O-HA
Ub-K63O-HA
D
Vector
btr32-Flag
TRIP-Flag
SOCS3a-Flag
STING-HA
btr32
TRIP
SOCS3a
E
Cyp17a2-Myc
IB: Myc
F
btr32-Myc
G
H
btr32-GFP
DsRed
Merge
ER-DsRed
Green-btr32
Red-N1
Red-ER
Intensity
Distance (μM)
I
mCherry
STING-mCherry
Cyp17a2-mCherry
Red-mCherry
Red-STING
Red-Cyp17a2
J
Pearson's correlation coefficient
btr32-GFP+mCherry
btr32-GFP+STING-mCherry
btr32-GFP+Cyp17a2-mCherry
K
btr32-HA
STING-Flag
Cyp17a2-Myc
L
STING+Vector
STING+Cyp17a2
IFNφ1pro. lucif. act.
Control
btr32
M
vig1
Rel. mRNA. Exp
N
Cyp17a2-HA
btr32-Flag
IB: STING
IB: Flag
IB: HA
IB: Actin

Figure 6

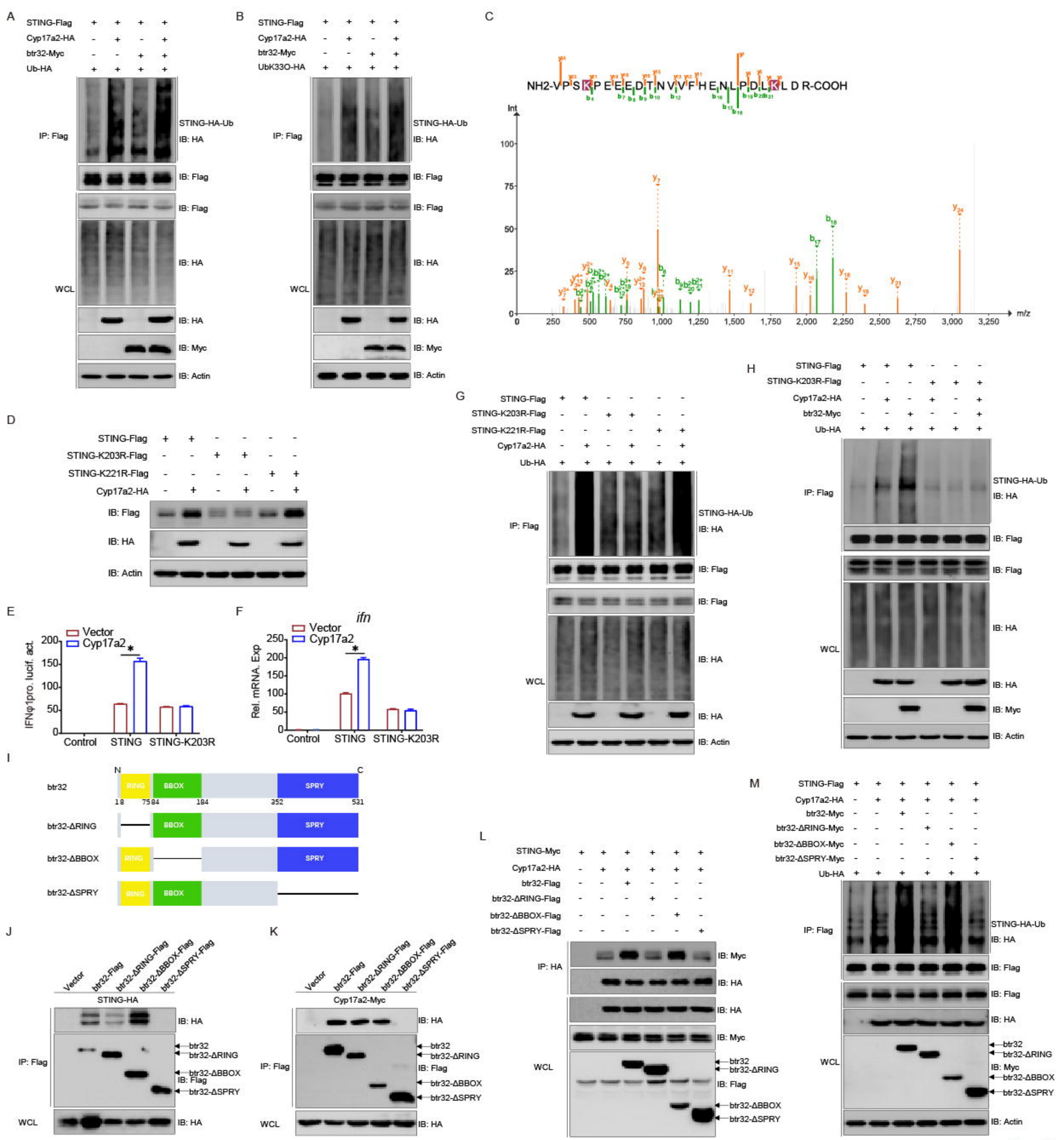
A
STING-Flag
Cyp17a2-HA
btr32-Myc
Ub-HA
IP: Flag
STING-HA-Ub
IB: HA
IB: Flag
WCL
IB: Myc
IB: Actin
B
UbK33O-HA
C
NH2-VPSKPEEEDTNVVFHENLPDLKLDR-COOH
Int
m/z
D
STING-K203R-Flag
STING-K221R-Flag
E
Vector
Cyp17a2
IFNφ1pro. lucif. act.
Control
STING
STING-K203R
F
ifn
Rel. mRNA. Exp
G
H
I
btr32
RING
BBOX
SPRY
N
C
18
75
84
184
352
531
btr32-ΔRING
btr32-ΔBBOX
btr32-ΔSPRY
J
Vector
btr32-Flag
btr32-ΔRING-Flag
btr32-ΔBBOX-Flag
btr32-ΔSPRY-Flag
STING-HA
K
Cyp17a2-Myc
L
STING-Myc
btr32-Flag
btr32-ΔRING-Flag
btr32-ΔBBOX-Flag
btr32-ΔSPRY-Flag
M
btr32-Myc
btr32-ΔRING-Myc
btr32-ΔBBOX-Myc
btr32-ΔSPRY-Myc

Figure 7

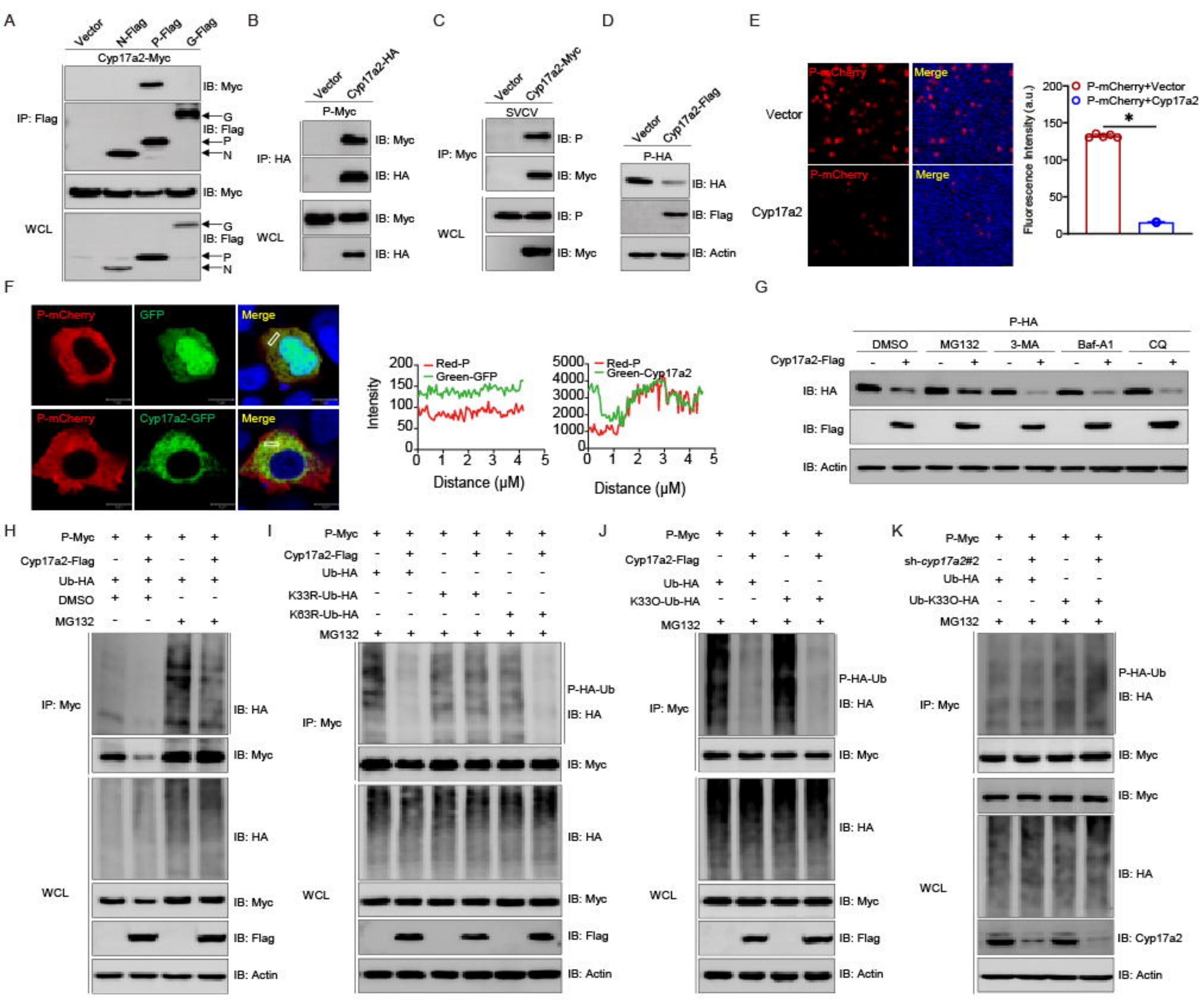
A
Vector
N-Flag
P-Flag
G-Flag
Cyp17a2-Myc
IP: Flag
IB: Myc
IB: Flag
G
P
N
WCL
B
Vector
Cyp17a2-HA
P-Myc
IP: HA
IB: Myc
IB: HA
WCL
C
Vector
Cyp17a2-Myc
SVCV
IP: Myc
IB: P
IB: Myc
WCL
D
Vector
Cyp17a2-Flag
P-HA
IB: HA
IB: Flag
IB: Actin
E
P-mCherry
Merge
Vector
Cyp17a2
P-mCherry+Vector
P-mCherry+Cyp17a2
Fluorescence Intensity (a.u.)
F
P-mCherry
GFP
Merge
Cyp17a2-GFP
Red-P
Green-GFP
Green-Cyp17a2
Intensity
Distance (μM)
G
P-HA
DMSO
MG132
3-MA
Baf-A1
CQ
Cyp17a2-Flag
IB: HA
IB: Flag
IB: Actin
H
P-Myc
Cyp17a2-Flag
Ub-HA
DMSO
MG132
IP: Myc
IB: HA
IB: Myc
WCL
IB: Flag
IB: Actin
I
K33R-Ub-HA
K63R-Ub-HA
P-HA-Ub
J
K33O-Ub-HA
K
sh-cyp17a2#2
Ub-K33O-HA
IB: Cyp17a2

Figure 8

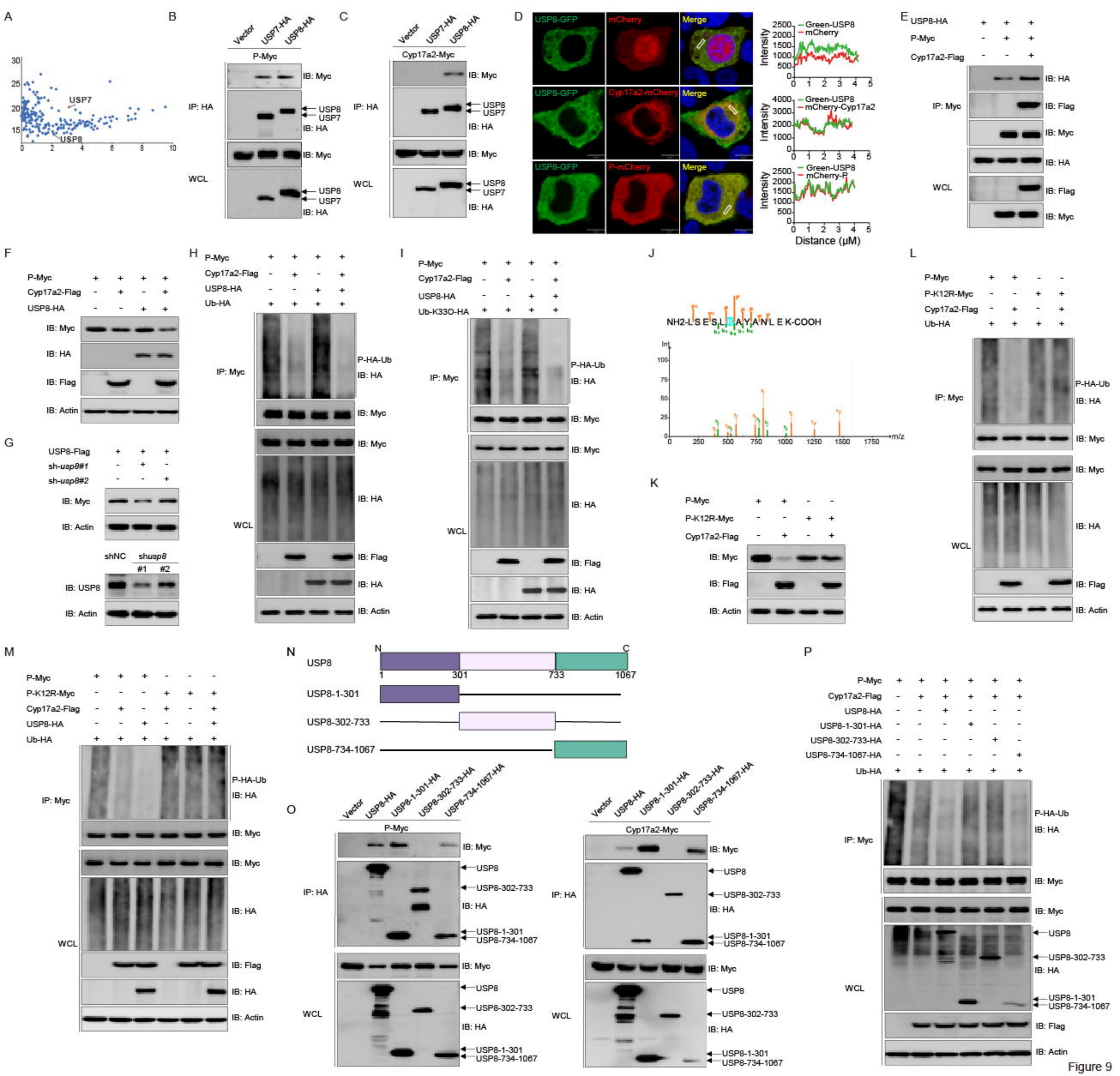
A
USP7
USP8
B
Vector
USP7-HA
USP8-HA
P-Myc
IB: Myc
IP: HA
USP8
USP7
IB: HA
WCL
C
Cyp17a2-Myc
D
USP8-GFP
mCherry
Merge
Cyp17a2-mCherry
P-mCherry
Green-USP8
mCherry-Cyp17a2
mCherry-P
Intensity
Distance (μM)
E
USP8-HA
P-Myc
Cyp17a2-Flag
IP: Myc
IB: Flag
F
IB: Actin
G
USP8-Flag
sh-usp8#1
sh-usp8#2
shNC
shusp8
#1
#2
IB: USP8
H
Ub-HA
P-HA-Ub
I
Ub-K33O-HA
J
NH2-L S E S L K A Y A N L E K-COOH
m/z
K
P-K12R-Myc
L
M
N
USP8
USP8-1-301
USP8-302-733
USP8-734-1067
O
P
USP8-1-301-HA
USP8-302-733-HA
USP8-734-1067-HA

Figure 9

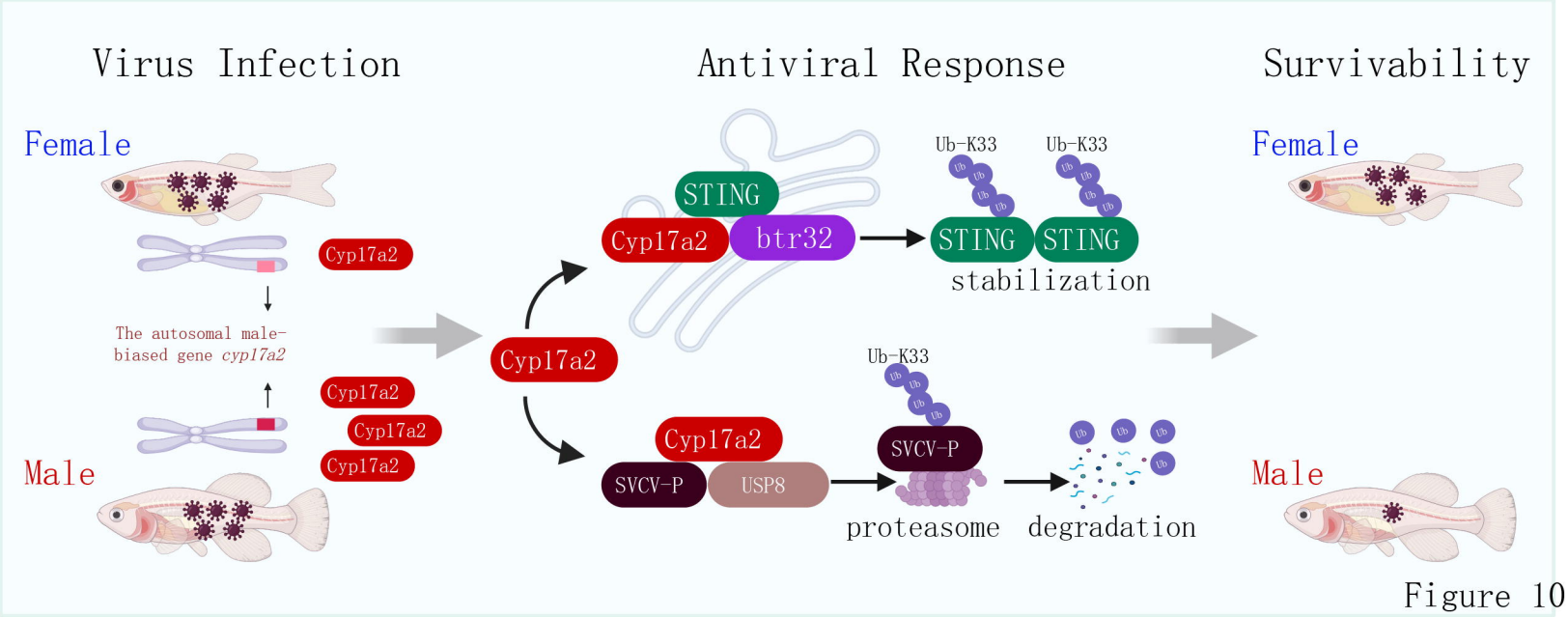
Virus Infection
Antiviral Response
Survivability
Female
Male
Cyp17a2
Cyp17a2
Cyp17a2
Cyp17a2
The autosomal male-biased gene cyp17a2
Cyp17a2
STING
Cyp17a2
btr32
Ub-K33
Ub-K33
STING
STING
stabilization
Cyp17a2
Cyp17a2
SVCV-P
USP8
Ub-K33
SVCV-P
proteasome
degradation
Female
Male

Figure 10